© 2018. Published by The Company of Biologists Ltd | Journal of Cell Science (2018) 131, jcs217331. doi:10.1242/jcs.217331

RESEARCH ARTICLE

The putative ceramide-conjugation protein Cwh43 regulates G0 quiescence, nutrient metabolism and lipid homeostasis in fission yeast

Norihiko Nakazawa[1,‡], Takayuki Teruya[1], Kenichi Sajiki[1], Kazuki Kumada[1], Alejandro Villar-Briones[1,*], Orie Arakawa[1], Junko Takada[1], Shigeaki Saitoh[2] and Mitsuhiro Yanagida[1,‡]

ABSTRACT

Cellular nutrient states control whether cells proliferate, or whether they enter or exit quiescence. Here, we report characterizations of fission yeast temperature-sensitive (ts) mutants of the evolutionarily conserved transmembrane protein Cwh43, and explore its relevance to utilization of glucose, nitrogen source and lipids. GFP-tagged Cwh43 localizes at ER associated with the nuclear envelope and the plasma membrane, as in budding yeast. We found that *cwh43* mutants failed to divide in low glucose and lost viability during quiescence under nitrogen starvation. In *cwh43* mutants, comprehensive metabolome analysis demonstrated dramatic changes in marker metabolites that altered under low glucose and/or nitrogen starvation, although *cwh43* cells apparently consumed glucose in the culture medium. Furthermore, we found that *cwh43* mutant cells had elevated levels of triacylglycerols (TGs) and coenzyme A, and that they accumulated lipid droplets. Notably, TG biosynthesis was required to maintain cell division in the *cwh43* mutant. Thus, Cwh43 affects utilization of glucose and nitrogen sources, as well as storage lipid metabolism. These results may fit a notion developed in budding yeast stating that Cwh43 conjugates ceramide to glycosylphosphatidylinositol (GPI)-anchored proteins and maintains integrity of membrane organization.

KEY WORDS: Cwh43, Ceramide, Fission yeast, Low glucose, Nitrogen starvation, Lipid droplet

INTRODUCTION

Nutrition is a major determinant of whether cells divide or undergo cell cycle arrest to enter quiescence. Principal nutrients include carbohydrates, proteins and lipids, although vitamins and minerals are also essential. Carbohydrates are hydrolyzed to monosaccharides, such as glucose, the essential carbon and energy source for all organisms. Amino acids are a critical nitrogen source for synthesis of numerous biological substances, such as proteins, nucleotides and neurotransmitters, and are also necessary for gluconeogenesis under low-glucose conditions. Under environmental conditions in which carbon and/or nitrogen sources are not available, cells have the ability to utilize lipids as an alternative energy source. Most eukaryotic cells are capable of storing lipid droplets (LDs), comprised primarily of triacylglycerols (TGs) and sterols, in specialized intracellular organelles (Meyers et al., 2017; Pol et al., 2014; Thiam et al., 2013). Remarkably, changes in the cellular regulation of LDs and LD-associated proteins are linked to human diseases including obesity, diabetes and atherosclerosis (Krahmer et al., 2013). Therefore, metabolic processes involving principal nutrients are tightly integrated.

Mechanisms controlling metabolism of principal nutrients are assumed to be evolutionarily conserved. Because the fission yeast *Schizosaccharomyces pombe* is a suitable model organism for the study of cell division and quiescence, we investigated genetically controlled mechanisms in this organism that respond to fasting or starvation. Nitrogen starvation induces entry into the quiescent G0 phase, in which cells remain alive for months without growth or division (Su et al., 1996; Yanagida, 2009), demonstrating *S. pombe* G0 quiescence provides a model system to study chronological lifespan. Using a collection of temperature-sensitive (ts) mutants, we identified more than 80 'super housekeeping genes' required for both proliferation and nitrogen starvation-induced G0 quiescence (Sajiki et al., 2009 and our unpublished data). For example, the stress-responsive mitogen-activated protein kinase (MAPK) Sty1 is required for G0 entry. The 26S proteasome maintains G0 quiescence by minimizing reactive oxygen species (ROS) in collaboration with autophagy (Takeda et al., 2010). By contrast, the quiescent state has also been studied under limited glucose conditions. In media containing low glucose (4.4 mM, 0.08%), *S. pombe* wild-type cells are able to divide as well as in normal glucose media (111 mM, 2%). It is reported that the critical glucose transporter Ght5, the zinc-finger transcription factor Scr1, the calmodulin kinase kinase (CaMKK)-like Ssp1, the PP2A phosphatase inhibitor Sds23 and the TORC2-mediated signaling pathway are essential for cell division under low-glucose conditions (Hanyu et al., 2009; Saitoh et al., 2015). In response to a wide range of environmental stresses, a limited number of key signaling pathways including protein kinase C (PKC) (Levin et al., 1990; Toda et al., 1993), MAPKs (Chen and Thorner, 2007; Perez and Cansado, 2010; Shiozaki and Russell, 1995; Sugiura et al., 1999, 1998) and the Ca^{2+}/calmodulin-dependent phosphatase calcineurin (Cyert, 2003; Sugiura et al., 2002; Yoshida et al., 1994), become activated. Thus, identification of factors involved in utilization of both carbon and nitrogen sources should help to illuminate common signaling pathways of principal nutrients.

In this study, we isolated eight temperature-sensitive (ts) mutant alleles of the fission yeast *cwh43* gene from our ts mutant collections, and found that seven of these mutants showed sensitivity to both nitrogen starvation and glucose limitation. Cwh43 encodes a conserved transmembrane protein that is thought

[1]G0 Cell Unit, Okinawa Institute of Science and Technology Graduate University, Tancha 1919-1, Onna-son, Okinawa 904-0495, Japan. [2]Institute of Life Science, Kurume University, Hyakunen-Kohen 1-1, Kurume, Fukuoka 839-0864, Japan. *Present address: Okinawa Institute of Science and Technology Graduate University, Instrumental Analysis Section, Tancha 1919-1, Onna-son, Okinawa, Japan 904-0495.

‡Authors for correspondence (nakazawa@oist.jp; myanagid@gmail.com)

N.N., 0000-0001-8386-0812; M.Y., 0000-0003-0293-5654

Received 1 March 2018; Accepted 20 July 2018

Journal of Cell Science (2018) 131, jcs217331. doi:10.1242/jcs.217331

to incorporate the sphingolipid, ceramide, into a lipid moiety of glycosylphosphatidylinositol (GPI)-anchored proteins (GPI-APs) in budding yeast plasma membranes (Ghugtyal et al., 2007; Martin-Yken et al., 2001; Reggiori et al., 1997; Umemura et al., 2007; Yoko-o et al., 2013). Ceramide is present in all eukaryotic cells and serves structural functions in lipid bilayers (Chaurasia and Summers, 2015). In addition, ceramide acts as a signaling molecule in response to stresses such as UV irradiation and chemotherapy, which induce cell cycle arrest, apoptosis and cell senescence (Hannun, 1996; Hannun and Obeid, 2008). To address the novel, nutrient-related phenotypes in *S. pombe cwh43* mutant cells, we comprehensively measured the levels of metabolites and lipids using metabolomic and lipidomic approaches. Strikingly, Cwh43-deficient cells had changed levels of nutrient stress-inducible metabolic compounds and they also over-accumulated TGs (neutral lipids) in LDs. We present evidence that Cwh43, a putative ceramide-conjugation protein, is intimately involved in cellular metabolism of principal nutrients and storage lipids.

RESULTS

Isolation of *S. pombe cwh43* temperature-sensitive mutants

We previously developed 1015 ts haploid *S. pombe* strains (Hayashi et al., 2004), and identified genes responsible for their ts phenotypes (Hanyu et al., 2009; Hayashi et al., 2004; Nakamura et al., 2012). To identify the mutant gene, plasmids that rescued the ts phenotype of the mutant strain were isolated by transformation, using an *S. pombe* genomic DNA library. Plasmid DNAs recovered from Ts^+ transformants were then subcloned and sequenced. Nevertheless, the colony number of obtained transformants was occasionally insufficient to identify the high-copy suppressor gene owing to low plasmid transformation efficiency. To overcome this technical difficulty for determination of mutation sites in eight ts mutant strains (ts200, ts202, ts285, ts609, ts724, ts824, ts833, ts941), we performed whole-genome sequencing of the mutant strains. Upon completion, all mutation sites responsible for these eight ts phenotypes turned out to be located in *cwh43*$^+$ (SPAC589.12), encoding the putative glycosylceramide biosynthesis protein Cwh43 (PomBase, https://www.pombase.org/) (Fig. 1A). We backcrossed these ts strains with the wild-type multiple times and confirmed that the amino acid changes co-segregated with the ts phenotypes.

Cwh43 is a conserved eukaryotic transmembrane protein. It contains the Frag1/DRAM/Sfk1 family domain at its N-terminus and an endonuclease/exonuclease/phosphatase superfamily domain at its C-terminus (Dlakić, 2000; Ghugtyal et al., 2007; Martin-Yken et al., 2001; Umemura et al., 2007) (Fig. 1A). Nineteen transmembrane helix motifs occur in the N-terminal 700 amino acids. The mutation sites of four *cwh43* ts mutants, K273stop (ts609), G300E (ts824), N418K (ts285) and W605stop (ts202), are

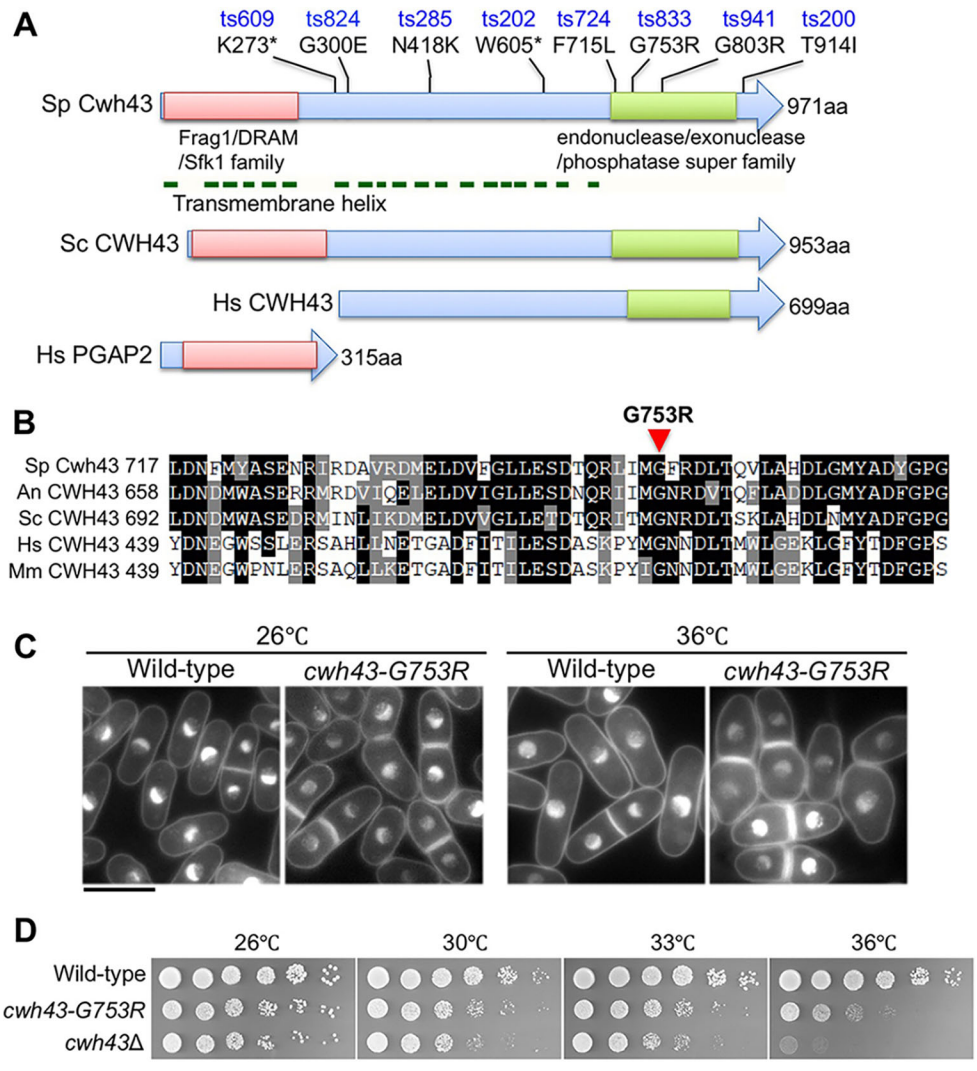

Fig. 1. Isolation of *S. pombe* temperature-sensitive mutants of the gene encoding the conserved transmembrane protein Cwh43. (A) *S. pombe* Cwh43 (Sp Cwh43) is drawn schematically along with *S. cerevisiae* CWH43 (Sc CWH43) protein. Mutation sites of eight *S. pombe cwh43* ts mutants are indicated with amino acid changes. Asterisks indicate stop codons. The N- and C-terminal conserved regions of the Frag1/DRAM/Sfk1 and endonuclease/exonuclease/phosphatase superfamilies are indicated with red and green boxes, respectively. Horizontal green lines show positions of transmembrane helices in Sp Cwh43 protein. Cwh43 comprises two distinct proteins in mammalian cells. Human PGAP2 and CWH43/FLJ21511 are homologous to the N- and C-terminal regions of yeast Cwh43, respectively (Ghugtyal et al., 2007; Umemura et al., 2007). (B) Amino acid sequences of the conserved C-terminal regions that surround the G753R mutation in the *S. pombe cwh43-833* ts strain. Amino acid sequences of Cwh43 orthologs in *S. pombe* (Sp), *Aspergillus niger* (An), *Saccharomyces cerevisiae* (Sc), *Homo sapiens* (Hs), and *Mus musculus* (Mm) are aligned. (C) DAPI-stained wild-type and *cwh43-G753R* mutant cells are shown. Mild and severe defects in cell morphology were observed in *cwh43-G753R* mutant cells at 26°C and 36°C for 6 h, respectively. Scale bar: 10 µm. (D) Wild type, the *cwh43-G753R* mutant and the deletion mutant lacking the *cwh43*$^+$ gene (*cwh43*Δ) were spotted on EMM2 solid medium.

Journal of Cell Science (2018) 131, jcs217331. doi:10.1242/jcs.217331

located in the region that contains transmembrane motifs. In the C-terminal domain, the evolutionarily conserved F715, G753 and G803 were mutated to leucine (ts724), arginine (ts833) and arginine (ts941) residues, respectively (Fig. 1B; Fig. S1). T914I (ts200) is located just behind the C-terminal domain. In contrast, none of our mutants resulted from mutations in the conserved N-terminal domain of the Frag1/DRAM/Sfk1 family. Thus, the transmembrane region and conserved C-terminal domain appear to be indispensable for *S. pombe* Cwh43 function, although the N-terminal domain may have an additive role, consistent with the more-severe phenotype of the deletion mutant of the full-length *cwh43*$^{+}$ gene (see below).

Construction of *cwh43-G753R* and *cwh43*Δ mutant strains

All eight *cwh43* mutants produced partly elongated, swollen cell shapes at the permissive temperature (26°C), and this morphological abnormality was more severe at the restrictive temperature (36°C) (Fig. 1C; Fig. S2A). Abnormal cell morphology was indistinguishable among the eight mutant strains. We selected the G753R mutation (ts833) for further phenotypic analyses. It is located in the C-terminally conserved region and loses viability in vegetative and G0 quiescent cells (see below).

To confirm that the ts phenotype is caused by single amino acid changes in the Cwh43 protein, we introduced the G753R mutation into the wild-type strain under the native promoter, along with the hemagglutinin (HA) tag. The resulting transformants, designated Cwh43-WT-HA:KanR and *cwh43-G753R*-HA:KanR (hereafter, termed wild type and *cwh43-G753R*, respectively), were used in this study. The HA-tagged wild-type strain showed normal cell growth, as did the non-tagged wild-type; however, the *cwh43-G753R* mutant and the original *cwh43-833* mutant failed to form colonies at the restrictive temperature (36°C) (Fig. 1D; Fig. S2B). After the temperature shift from 26°C to 36°C, the cell count of the *cwh43-G753R* mutant hardly increased, while viability decreased from 55% to 20% (Fig. S2C). Thus, cell number increase and viability of *cwh43-G753R* mutant cells were impaired at 36°C. The cell morphological defect was evident even at 26°C, suggesting that the cell morphological abnormality itself was not a lethal attribute. The proportion of cells with septa was significantly higher in the *cwh43-G753R* mutant at both 26°C and 36°C, while the numbers with multiple septa increased at 36°C, suggesting that this mutant is defective in cytokinesis (Fig. S2D). These phenotypes of the integrated strain were indistinguishable from those of the original *cwh43-833* mutant.

Next, we constructed a deletion mutant of the *cwh43*$^{+}$ gene by replacing it with the hygromycin-resistance gene. The resulting *cwh43* deletion mutant (*cwh43*Δ) failed to form colonies at 36°C, as did the *cwh43-G753R* ts mutant (Fig. 1D), indicating that deletion of *cwh43*$^{+}$ is indispensable for cell proliferation at high temperature. The colony-forming capacity of the *cwh43*Δ mutant is less than that of the *cwh43-G753R* mutant at all tested temperatures. Consistent with this, the morphological abnormality of the *cwh43Δ* mutant was more severe than that of the *cwh43-G753R* mutant at both 26°C and 36°C (Fig. S2E). Thus, *cwh43-G753R* mutant cells may be not fully devoid of Cwh43 function.

Monitoring defective cytokinesis in living *cwh43* mutant cells

To examine cell division of *cwh43-G753R* mutant cells in detail, we made time-lapse observations of living cells. Wild-type and *cwh43-G753R* cells were cultivated at 26°C and then observed using a microfluidic perfusion system at 26°C or 36°C (Materials and Methods). At 26°C, DIC images showed that most wild-type cells divided within 4 h, and septum formation occurred in one or two movie frames (15–30 min) just before cell division (Fig. 2A, top; Movie 1). However, in the *cwh43* mutant, cell division required 2 to 8 h and septum formation took >2 h, demonstrating that completion of cytokinesis was significantly delayed (Fig. 2A, bottom; Movie 2). After the temperature shift to 36°C, division of *cwh43-G753R* mutant cells was blocked but this did not occur in wild-type cells (Fig. 2B; Movies 3,4). Mutant cells gradually became elongated and swelled without cell division, resulting in multiple septa and protrusion of cytosol. In addition, Aniline Blue staining of *cwh43-G753R* mutant cells showed abnormally high concentrations of the cell wall component 1,3-β-glucan, particularly at the septum, compared with dividing wild-type cells (Fig. 2C). This abnormal accumulation of 1,3-β-glucan was obvious at 36°C. As reported in a large number of mutant strains defective in cell wall integrity, the ts phenotype of *cwh43* mutant cells was suppressed in the presence of the osmotic stabilizer sorbitol (1.2 M) (Fig. S2F). Concomitantly, the glucan accumulation phenotype was slightly alleviated by sorbitol treatment (Fig. S2G), implying a correlation between cell wall defects and excessive glucan deposition. Taken together, these data indicate that impaired Cwh43 delayed completion of cytokinesis, presumably by causing excess 1,3-β-glucan to accumulate at the septum.

cwh43 mutant shows low-glucose sensitivity and improper localization of glucose transporters, in spite of glucose consumption from the culture medium

To test whether the *cwh43*$^{+}$ gene is required for cell proliferation under nutrient deficiency, we examined the colony-forming ability of *cwh43-G753R* mutant cells on solid EMM2 medium containing 0.04–2% glucose (2.2-111 mM; low to high levels of glucose). As previously described for the authentic low-glucose-sensitive mutant strains defective in Ssp1 kinase (Hanyu et al., 2009) and for a deletion mutant of hexose transporter Ght5 (Saitoh et al., 2015), the *cwh43-G753R* mutant failed to form colonies on low-glucose media (0.04–0.08%) at 26–33°C (Fig. 3A). Seven of the eight *cwh43* original ts mutant strains failed to divide under low-glucose conditions, exhibiting the low-glucose sensitivity (LGS) phenotype (Table S1).

Under low-glucose conditions, expression of specific hexose transporters is induced, and these transporters localize at the cell surface (Saitoh et al., 2015). We examined intracellular localization of the GFP-tagged hexose transporter Ght5 in *cwh43* mutant cells. After a shift from 2% to 0.08% glucose at 26°C, Ght5–GFP localization at the cell surface was not intense and showed cytoplasmic signals in the mutant (Fig. 3B). Expression of Ght5–GFP itself was properly induced in *cwh43* mutant cells, as well as in wild-type cells (Fig. 3C). In wild-type cells, another GFP-tagged hexose transporter, Ght8, was located at the plasma membrane exclusively at the poles of the cells (Saitoh et al., 2015) (Fig. S3). By contrast, *cwh43* mutant cells showed cytoplasmic accumulations of Ght8–GFP similar to those of Ght5-GFP, suggesting that Cwh43 affects the localization of hexose transporters under glucose limitation.

To examine glucose consumption by wild-type and *cwh43* mutant cells, we measured glucose concentrations in the culture medium. Cells initially cultivated in high-glucose (2%) medium were transferred to high (2%)- or low (0.08%)-glucose medium and incubated at 26°C, along with *ght5* deletion mutant cells (*ght5Δ*) as a control (Saitoh et al., 2015). Unexpectedly, glucose consumption was not significantly decreased in *cwh43* mutant cultures compared with wild-type, in either high or low glucose (Fig. 3D), although the cell number increase of *cwh43* mutant was decidedly slow (Fig. 3E).

Journal of Cell Science (2018) 131, jcs217331. doi:10.1242/jcs.217331

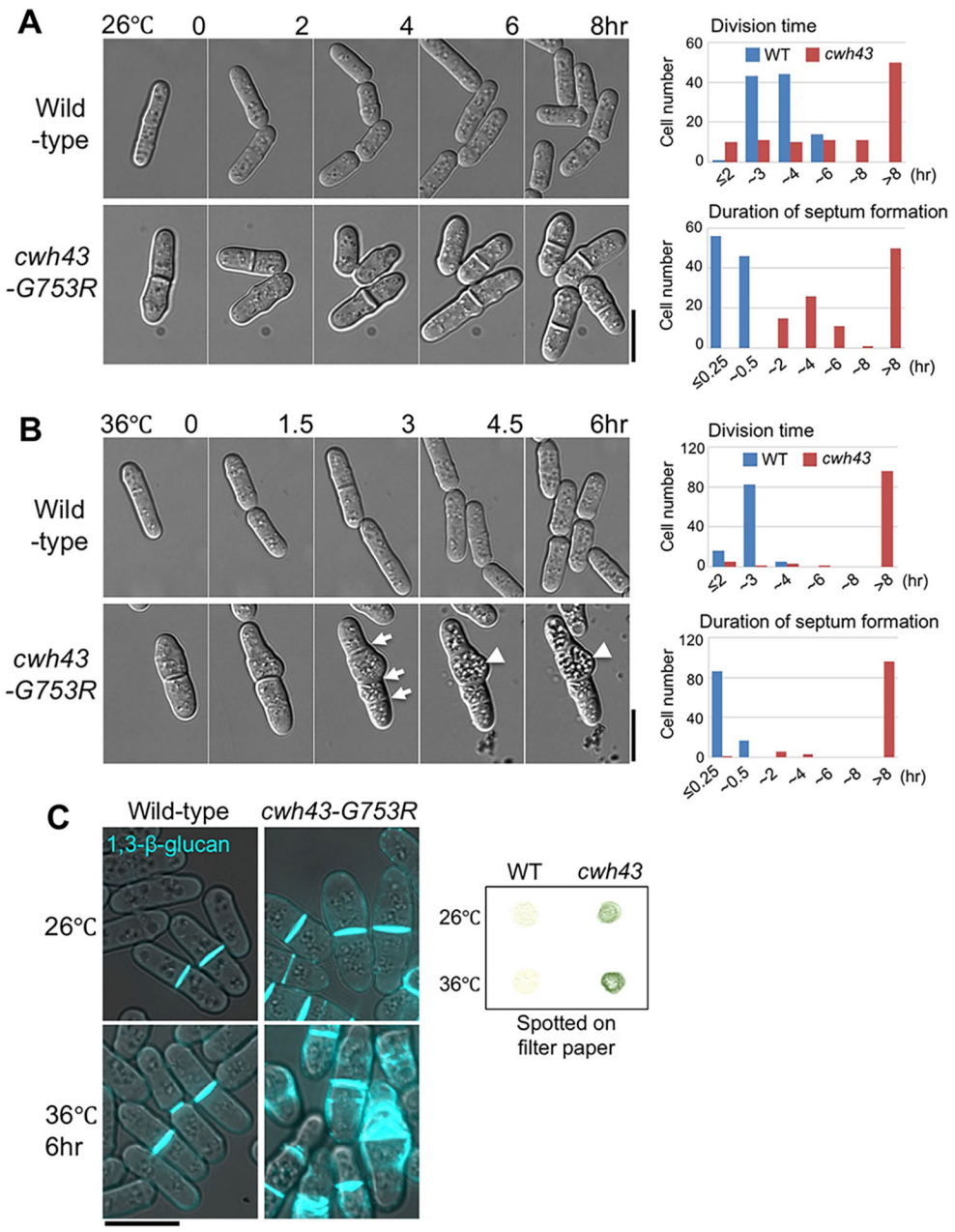

Fig. 2. Monitoring defective cytokinesis and excessive β-glucan accumulation at cell septa in *cwh43* mutant cells. (A,B) Left, time-lapse images of wild-type and *cwh43-G753R* strains. Cells were first cultivated at 26°C, and then either incubated further at 26°C (A) or shifted to 36°C (B) in a microfluidic perfusion chamber with a continuous supply of EMM2 medium. Differential interference contrast (DIC) images were presented at 2-h intervals (also see Movies 1–4). Arrows and arrowheads in B indicate the positions of multiple septa and a protruded cytosolic structure in *cwh43-G753R* cells, respectively. Right, division time and duration of septum formation were monitored for individual cells. (C) Left, fluorescence and bright-field images of wild-type and *cwh43-G753R* cells were captured after staining for the cell wall component 1,3-β-glucan using the fluorescent dye Aniline Blue. Cells were cultured at 26°C or 36°C for 6 h in liquid medium. Right, Aniline Blue-stained cells were spotted on filter paper. Scale bars: 10 µm.

These data suggest that the *cwh43* mutant consumes glucose in culture media, even if cell division is declined. Although subcellular localization of Ght5 and Ght8 were affected in the *cwh43* mutant, these transporters, which were partially retained at the plasma membrane, may be sufficient for glucose uptake.

Cwh43 is required to maintain cell viability during G0 quiescence induced by nitrogen starvation

We next determined whether the *cwh43*$^{+}$ gene is required for maintaining viability during G0 quiescence under nitrogen starvation. Wild-type and *cwh43-G753R* mutant cells grown in EMM2 medium (EMM2+N) were transferred to nitrogen-deficient EMM2-N at 26°C for 1 and 4 days, and the resulting quiescent G0 cells were spotted onto YPD solid medium in order to count the cells that were able to form colonies. In comparison with the wild type, under nitrogen starvation, the viability of *cwh43-G753R* mutants plunged to 27% after 1 day and to only 5% after 4 days, indicating severe defects in regeneration capacity, even after replenishment of the nitrogen source (Fig. 3F). The cell number of wild-type cells increased 3.7× after 1 day under nitrogen starvation, indicating that two rounds of cell division occurred. In contrast, numbers of *cwh43* mutant cells increased only 1.5×. Wild-type *S. pombe* cells have a spherical shape during G0 quiescence (Sajiki et al., 2009; Su et al., 1996); however, *cwh43-G753R* mutant cells presented non-spherical, deformed shapes (Fig. 3G). Six of the seven remaining *cwh43* ts mutant strains also decreased in viability under nitrogen starvation (Table S1). These results suggest that *cwh43* mutant cells failed to enter a normal and viable G0 quiescence in response to nitrogen deficiency.

Intracellular localization of Cwh43

To observe the intracellular localization of Cwh43 protein, the C-terminus of *cwh43*$^{+}$ or *cwh43-G753R* mutant genes was tagged with GFP. At 26°C, Cwh43-WT–GFP apparently localized at the nuclear membrane and the plasma membrane, accompanying

Journal of Cell Science (2018) 131, jcs217331. doi:10.1242/jcs.217331

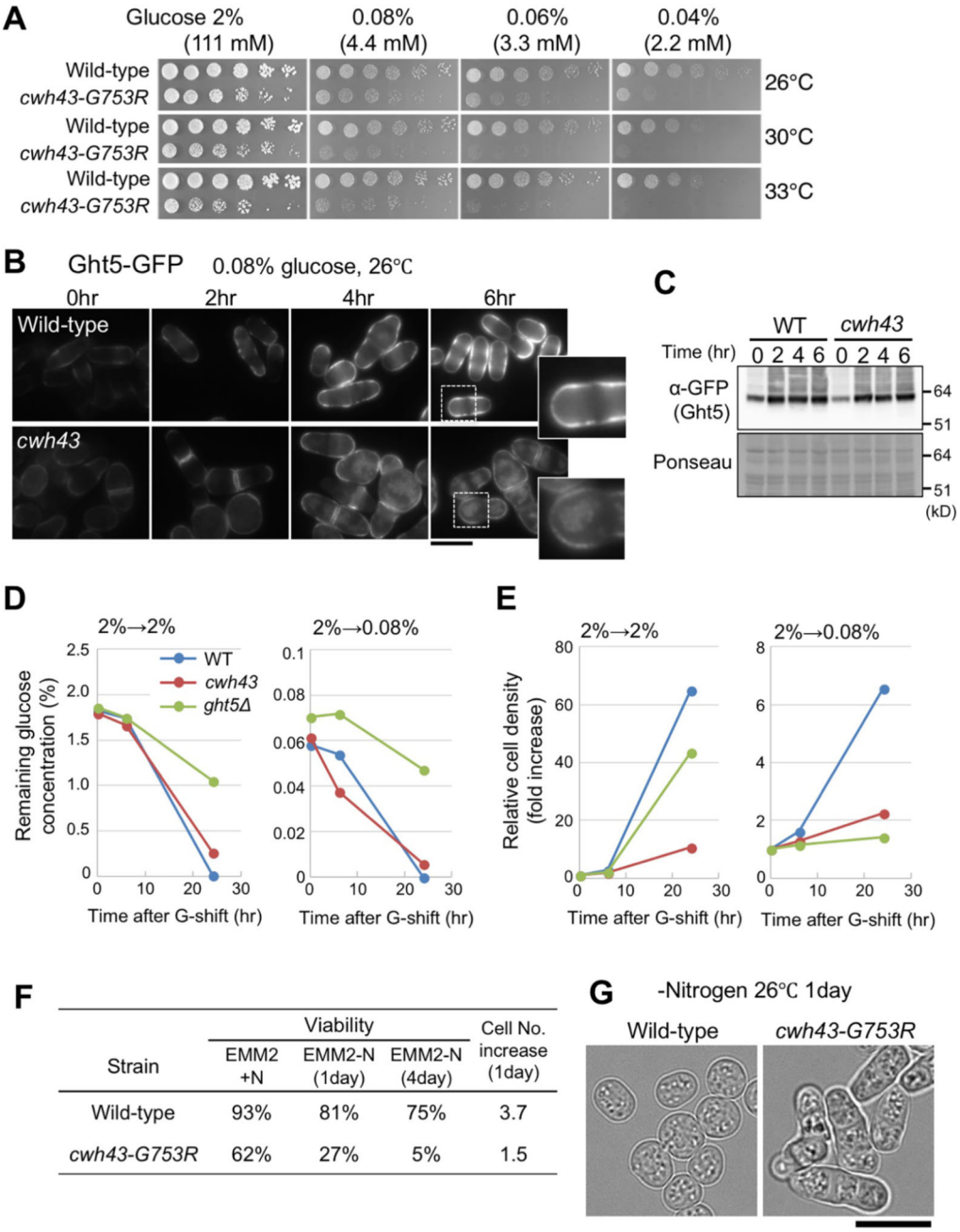

Strain	Viability EMM2 +N	Viability EMM2-N (1day)	Viability EMM2-N (4day)	Cell No. increase (1day)
Wild-type	93%	81%	75%	3.7
cwh43-G753R	62%	27%	5%	1.5

Fig. 3. *cwh43* mutants are sensitive to both low glucose and nitrogen starvation. (A) Aliquots (5×10^4 cells) of wild-type and *cwh43-G753R* strains were serially diluted 5×, spotted onto EMM2 medium containing the indicated concentrations (mM and percentage) of glucose at 26–33°C. (B) Expression and localization of GFP-tagged Ght5 in wild-type (top) and *cwh43-G753R* (bottom) mutant cells. Cells were cultivated in EMM2 liquid medium at 26°C and the glucose concentration was switched from 111 to 4.4 mM at time 0 h. GFP fluorescence microscopy images were taken at 2-h intervals. Inserts correspond to the areas of the white dashed boxes. (C) The protein level of Ght5–GFP was measured by immunoblotting. Total protein stained with Ponceau S is shown as a loading control. (D) Glucose consumption was examined in the wild-type, *cwh43* and *ght5Δ* mutant strains. Cells were transferred to fresh EMM2 supplied with 2% (left) or 0.08% (right) glucose (G-shift) at time 0 and cultivated at 26°C. The glucose concentration remaining in the medium was measured after 0, 6 and 24 h. Mean of two independent experiments are shown. (E) Cell proliferation was examined for the same conditions as in D. (F) Cell viability was measured at 1 and 4 days after nitrogen starvation (EMM2-N) at 26°C along with changes in cell number after 1 day. (G) Bright-field images of wild-type and *cwh43-G753R* mutant cells cultured after 1 day in EMM2-N medium at 26°C. Mutant cells showed non-spherical, deformed cell shapes. Scale bars: 10 µm.

granule-like cytoplasmic signals (Fig. 4A, top). At 36°C, localization of Cwh43–GFP was similar to that at 26°C, although GFP-tagged Cwh43 proteins were possibly unstable in high temperature, unlike the HA-tagged proteins (Fig. S4A,B). GFP-tagged Cwh43-G753R mutant proteins also showed similar localization as observed in wild type at both temperatures, implying that the G753R mutation does not affect Cwh43 localization itself (Fig. 4A, bottom; Fig. S4A). We also demonstrated that Cwh43–GFP localized in close proximity to plasma membranes by performing a protoplast preparation with enzymatic digestion of cell walls (Fig. 4B).

In budding yeast, CWH43 protein is reported to localize at the endoplasmic reticulum (ER) (Umemura et al., 2007). Considering that the ER is continuous with the nuclear envelope and is associated with the plasma membrane (Pidoux and Armstrong, 1993; Zhang et al., 2010), *S. pombe* Cwh43 proteins are also predicted to enrich in the ER. To test this possibility, we observed Cwh43–GFP localization in an *scs2Δ scs22Δ* double-deletion mutant strain in which the cortical ER dissociates from plasma membrane (Zhang et al., 2012). In wild-type cells, the Cwh43–GFP signals colocalized with the artificial luminal ER marker AHDL–mCherry (Zhang et al., 2010) at the plasma membrane and nuclear periphery (Fig. 4C, top). However, in *scs2Δ scs22Δ* double deletion mutant cells, localization of both Cwh43–GFP and AHDL–mCherry at the plasma membrane disappeared, and, instead, accumulated in the cytoplasm (Fig. 4C, bottom). This result indicates that Cwh43, as in budding yeast CWH43, enriches at ER associated with the plasma membrane.

Immunodetection of Cwh43 protein

Protein extracts of exponentially growing wild-type and *cwh43-G753R* strains were examined by immunoblotting using antibodies

Journal of Cell Science (2018) 131, jcs217331. doi:10.1242/jcs.217331

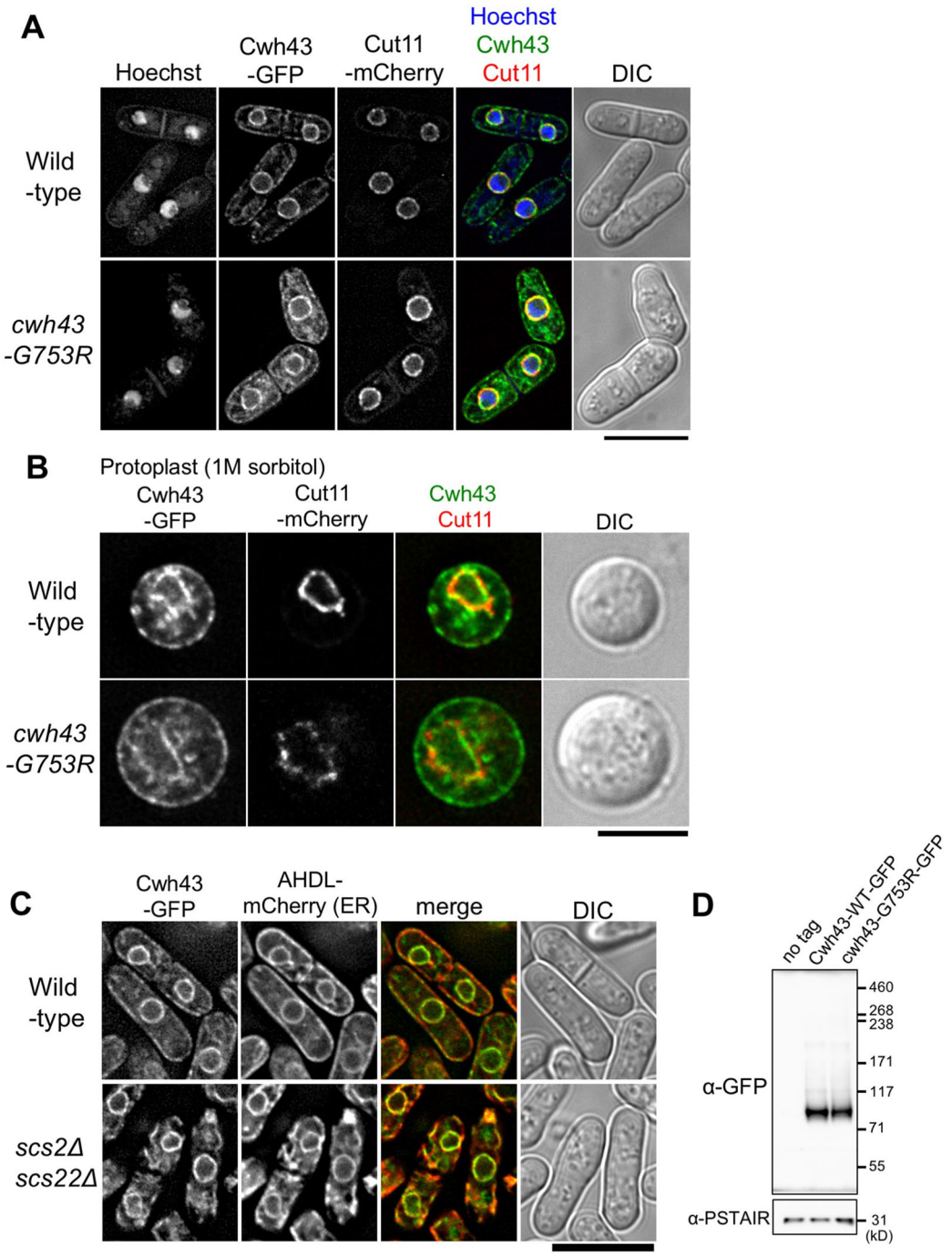

Fig. 4. GFP-tagged Cwh43 proteins localize at ER associated with the nuclear envelope and the plasma membrane. (A) Intracellular localization of GFP-tagged Cwh43-WT and -G753R proteins. Wild-type *cwh43*$^{+}$ or *cwh43-G753R* mutant genes were tagged with GFP and integrated into the chromosome under the native promoter with a kanamycin-resistance gene. The GFP-tagged *cwh43*$^{+}$ gene was functional, because the resulting integrant strain Cwh43-WT–GFP grew normally. These cells were cultivated at 26°C in EMM2 medium and fluorescence images were captured immediately without fixation. The nuclear envelope was visualized via mCherry-tagged Cut11 protein, a spindle pole body (SPB)-anchoring nuclear membrane protein (Broek et al., 1991; West et al., 1998), along with Hoechst 33342 staining for DNA and differential interference contrast (DIC) images. A single focal plane is shown. (B) Localization of Cwh43-WT–GFP or -G753R–GFP proteins in protoplasts. Cells were treated with a zymolyase and lysing enzyme mixture for 1 h in the presence of 1 M sorbitol and cells bearing both Cwh43–GFP and Cut11–mCherry were observed. A single focal plane is shown. (C) Localization of Cwh43–GFP and the artificial ER marker AHDL–mCherry in wild-type or *scs2Δ scs22Δ* double deletion mutant cells at 26°C. Scs2 and Scs22 link the cortical ER to the plasma membrane (Zhang et al., 2012). (D) Immunoblotting for GFP-tagged Cwh43-WT and -G753R proteins. Cells were cultivated at 26°C in EMM2 medium, and total protein extracts were prepared and subjected to SDS-PAGE. Levels of Cwh43-WT-GFP or -G753R–GFP proteins were examined by immunoblotting using an antibody against GFP, as well as a non-tagged control. Anti-PSTAIR antibody (against amino acid sequence of PSTAIR in Cdc2) was used as a loading control. Scale bars: 10 µm (A,C); 5 µm (B).

against HA or GFP. GFP- or HA-tagged Cwh43-WT and -G753R bands were observed at ∼71 kDa, which is less than their molecular masses (∼114 kDa for HA; ∼137 kDa for GFP) (Fig. 4D; Fig. S4C). Overproduction of chromosomally integrated Cwh43-WT protein tagged with HA at its N-terminus also showed bands at ∼71 kD (Fig. S4D, nmt-HA-Cwh43). In addition, overproduced Cwh43-

Journal of Cell Science (2018) 131, jcs217331. doi:10.1242/jcs.217331

WT–HA protein derived from *cwh43*$^{+}$ cDNA migrated faster than its expected molecular mass (Fig. S4D, pCwh43-HA). Hence, *S. pombe* Cwh43 presents a fast-migrating band in SDS-PAGE, a property often reported in ER- or membrane-associated proteins (Shirai et al., 2008).

Metabolic changes of biomarkers for nutrient stress in *cwh43* mutant cells

To further characterize the *cwh43* mutant phenotype, we applied our established metabolomic approach to *cwh43-G753R* mutant cells. Since cell viability of the *cwh43-G753R* mutant at 36°C and of the the *cwh43Δ* deletion mutant at both 26°C and 36°C was remarkably low, the *cwh43-G753R* strain was cultivated at 26°C in liquid EMM2 medium to mid-log phase (5×10^{6} cells/ml) along with wild-type cells, and these exponentially growing vegetative cells were collected. Then, cellular metabolites were extracted in 50% methanol and metabolites were analyzed using an LC-MS (LTQ Orbitrap mass spectrometer), as described previously (Pluskal et al., 2010b; Pluskal et al., 2011; see Materials and Methods). 119 metabolites were detected in wild-type and *cwh43-G753R* mutant strains (Fig. 5A; Table S2). In *cwh43* mutant cells, the levels of 26 metabolites increased more than 3-fold, while ten decreased more than 3-fold compared with wild-type cells (Fig. 5B, C; Table S3 and S4). Most of the compounds displaying significantly altered abundances in the mutant have been previously reported as marker metabolites that change under nitrogen starvation or low-glucose conditions (Fig. 5A) (Pluskal et al., 2011; Sajiki et al., 2013). The *cwh43* mutant also accumulated compounds that commonly change in both types of nutritional starvation.

The most strikingly accumulated compound in *cwh43* mutant cells was deferriferrichrome, which increased 19,000-fold relative to wild-type cells (Fig. 5B). Deferriferrichrome is an iron storage compound that increases with ferrichrome under low-glucose conditions (Pluskal et al., 2011). The iron-free form (deferri-form) of ferrichrome is produced under iron deficiency (Labbé et al., 2007; Schrettl et al., 2004), suggesting that *cwh43* mutant cells were deficient in iron.

Another group of drastically increased compounds includes ergothioneine and S-methyl-ergothioneine. Ergothioneine acts as a physiological antioxidant (Cheah and Halliwell, 2012) that has been reported to increase under both low-glucose and nitrogen starvation conditions (Pluskal et al., 2011; Sajiki et al., 2013). Hercynylcysteine sulfoxide is a precursor of ergothioneine. Consistent with the fact that ergothioneine is a sulfur-containing derivative of trimethyl histidine, tri- and di-methylated histidine also accumulated in *cwh43* mutant cells. Additionally, trehalose increased over 60-fold in the mutant. This compound is produced to stabilize proteins and membranes under various physiologic stresses, including heat shock, low glucose and nitrogen starvation (Cansado et al., 1998; Elbein et al., 2003; Pluskal et al., 2010b).

2-Oxoglutarate and succinate, intermediates of the TCA cycle, increased 89-fold and 6-fold, respectively, in *cwh43-G753R* mutant cells (Fig. 5B; Table S3). These compounds are specific biomarkers that increase during the nitrogen starvation response (Sajiki et al., 2013). By contrast, the purine biosynthesis pathway intermediates, 5-phospho-ribose 1-diphosphate (PRPP), aminoimidazole-4-carboxamide ribonucleotide (AICAR), N-succinocarboxamide-5-aminoimidazole ribonucleotide (SAICAR) and N-formylglycinamide ribonucleotide (FGAR) decreased remarkably in mutant cells (Fig. 5C; Table S4). These compounds have also been reported as marker metabolites that decrease immediately under nitrogen starvation (Sajiki et al., 2013). Taken together, the metabolomic analysis indicated that the *cwh43* mutant is apparently defective in utilization of both carbon and nitrogen sources, producing massive nutritional stresses, even when these nutrients are present in the culture medium.

In wild-type *S. pombe* cells, the level of free-form coenzyme A (CoA) is normally extremely low relative to other metabolites (Nakamura et al., 2012). However, in *cwh43* mutant cells, we found that the level of CoA increased more than 4000-fold compared to wild-type cells (Fig. 5A,B). This drastic increase in CoA content in the absence of Cwh43 function is a unique metabolic property that has not been reported under low glucose or nitrogen starvation. CoA is an essential cofactor in the metabolism of carboxylic acids and lipids, implying that *cwh43* mutant cells have altered lipid abundance.

cwh43 mutant cells overproduce triacylglycerols

To examine whether Cwh43 influences cellular lipid metabolism, we performed lipidomic analysis in wild-type and *cwh43-G753R* mutant cells. Cells were cultivated in EMM2 at 26°C and total lipids were extracted with tert-butylmethylether (Matyash et al., 2008). Lipid extracts were then subjected to LC/MS analysis and compounds were identified using Lipidomics Gateway Software (see Materials and Methods). We identified 124 lipids in both strains (Fig. 6A; Table S5). 15 lipids increased ≥3-fold in abundance while nine others diminished ≥3-fold in *cwh43-G753R* mutant cells compared to the wild type (Table S6). Notably, in mutant cells, 14 of 15 increased lipids were triacylglycerols (triglycerides, TGs) and the levels of 14 TG species were ∼3–5-fold higher than in wild-type cells (Fig. 6B). TG species containing unsaturated fatty acids increased, although TGs composed of only saturated fatty acids decreased in *cwh43* mutant (Fig. 6C).

Thin-layer chromatography (TLC) confirmed that TGs were enriched in *cwh43* mutant cells compared to wild-type cells (Fig. 6D). In *dga1Δ plh1Δ* double-mutant cells lacking the TG biosynthetic enzymes Dga1 and Plh1 (Meyers et al., 2016) (see below), TGs were not detected, as expected. Sterol esters also increased in *cwh43* mutant, though levels of diacylglycerols (DGs) were comparable to those in wild-type and *dga1Δ plh1Δ* mutant cells. Taken together, these results provide clear evidence that defects in Cwh43 function raise levels of TGs along with levels of sterol esters.

Lipid droplets accumulate in *cwh43-G753R* mutant cells

To further validate elevated levels of TGs in *cwh43* mutant cells, we stained them with BODIPY 493/503, a fluorescent dye that specifically binds to TGs, and we observed LDs, consisting of TGs and cholesterol (Long et al., 2012; Pol et al., 2014; Thiam et al., 2013). In *cwh43* mutants, the number and size of BODIPY-stained LDs was substantially greater than in wild-type cells (Fig. 6E–G), confirming that impaired function of Cwh43 causes excess accumulation of storage lipids in vegetative cells.

Next, we constructed deletion mutant strains of two TG synthesis enzymes, Dga1 and Plh1, to determine whether the increased number of LDs in *cwh43* mutant cells depends on TG synthetic pathways (Meyers et al., 2016). Both Dga1 (a diacylglycerol O-acyltransferase) and Plh1 (a phospholipid-diacylglycerol acyltransferase) conjugate acyl chains to diacylglycerol, using distinct acyl chain donors, acyl-CoA and glycerophospholipid, respectively (Oelkers et al., 2002, 2000; Zhang et al., 2003). As previously reported (Meyers et al., 2016), *dga1Δ plh1Δ* double mutant cells barely produce LDs (Fig. 6E,F). Furthermore, *cwh43-*

Journal of Cell Science (2018) 131, jcs217331. doi:10.1242/jcs.217331

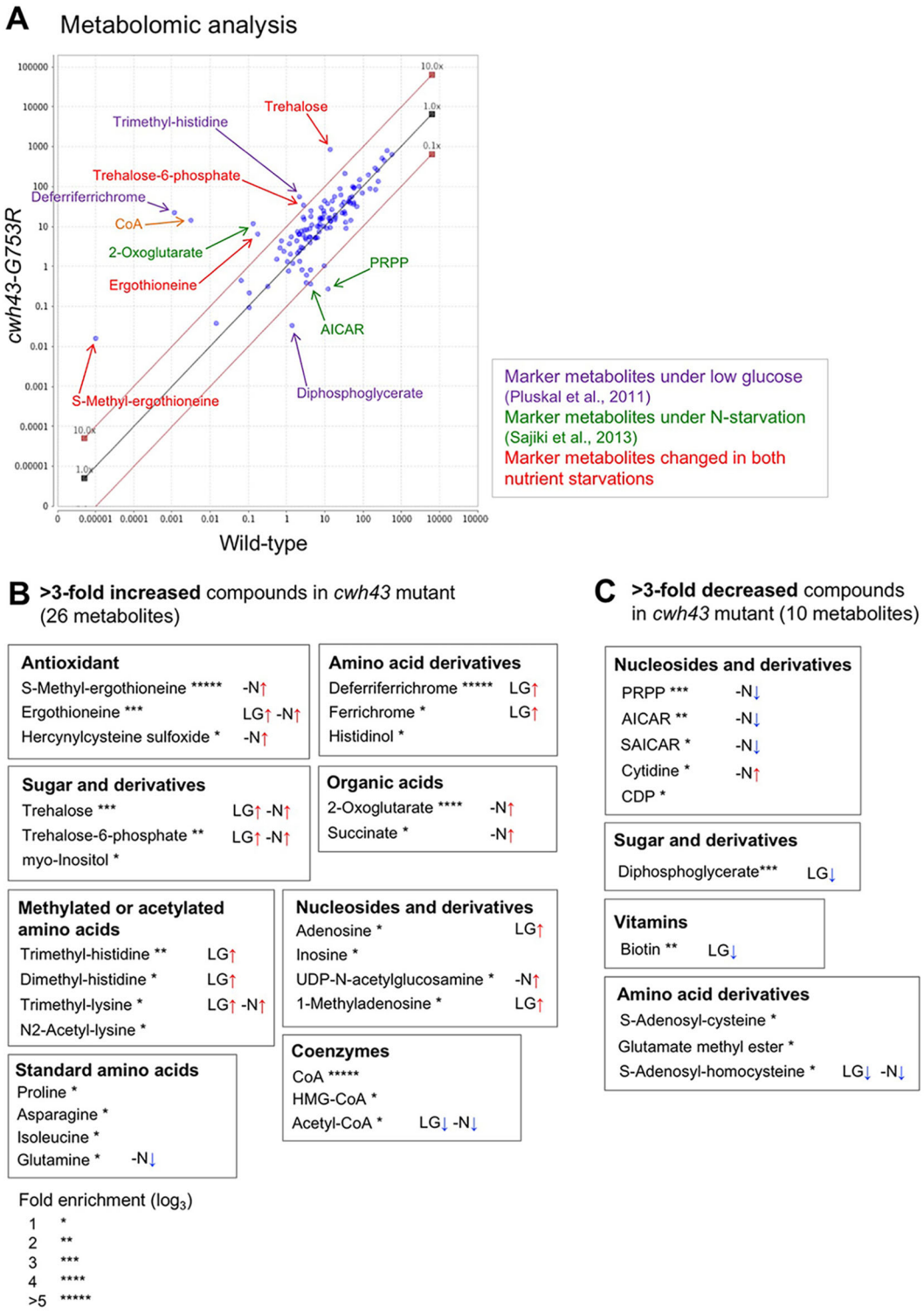

Fig. 5. Metabolic changes in nutritional starvation biomarkers in vegetative *cwh43* mutant cells. (A) Scatter plot comparing normalized peak areas of all 119 metabolites detected in wild-type and *cwh43-G753R* cells. Metabolites were extracted from exponentially growing vegetative cells at 26°C and analyzed using LC/MS. Compounds that increased or decreased >10-fold in *cwh43* mutant cells relative to wild-type are indicated by arrows. Marker metabolites specific for low glucose (Pluskal et al., 2011) and nitrogen starvation (Sajiki et al., 2013) are shown in purple and green, respectively. Metabolic compounds that changed in both low glucose and nitrogen starvation (Pluskal et al., 2010b; Pluskal et al., 2011; Sajiki et al., 2013) are indicated in red. CoA has not been reported as marker metabolite under both nutrient deficiencies previously (orange). (B,C) 26 metabolites increased more than 3-fold (B) and ten metabolites decreased more than 3-fold (C) in *cwh43* mutant cells compared with wild-type cells. The degree of increase or decrease in the ratio of each compound is shown with asterisks in the ternary logarithm. Compounds previously reported to increase (upward arrows) or decrease (downward arrows) under low glucose (LG) or nitrogen starvation (−N) are indicated. In *cwh43* mutant cells, antioxidants, deferriferrichrome, trehalose, TCA cycle intermediates, methylated amino acids and the free form of coenzyme A (CoA) substantially increased; however, purine biosynthesis intermediates, diphosphoglycerate and biotin, which reflect a high-energy state, decreased.

Journal of Cell Science (2018) 131, jcs217331. doi:10.1242/jcs.217331

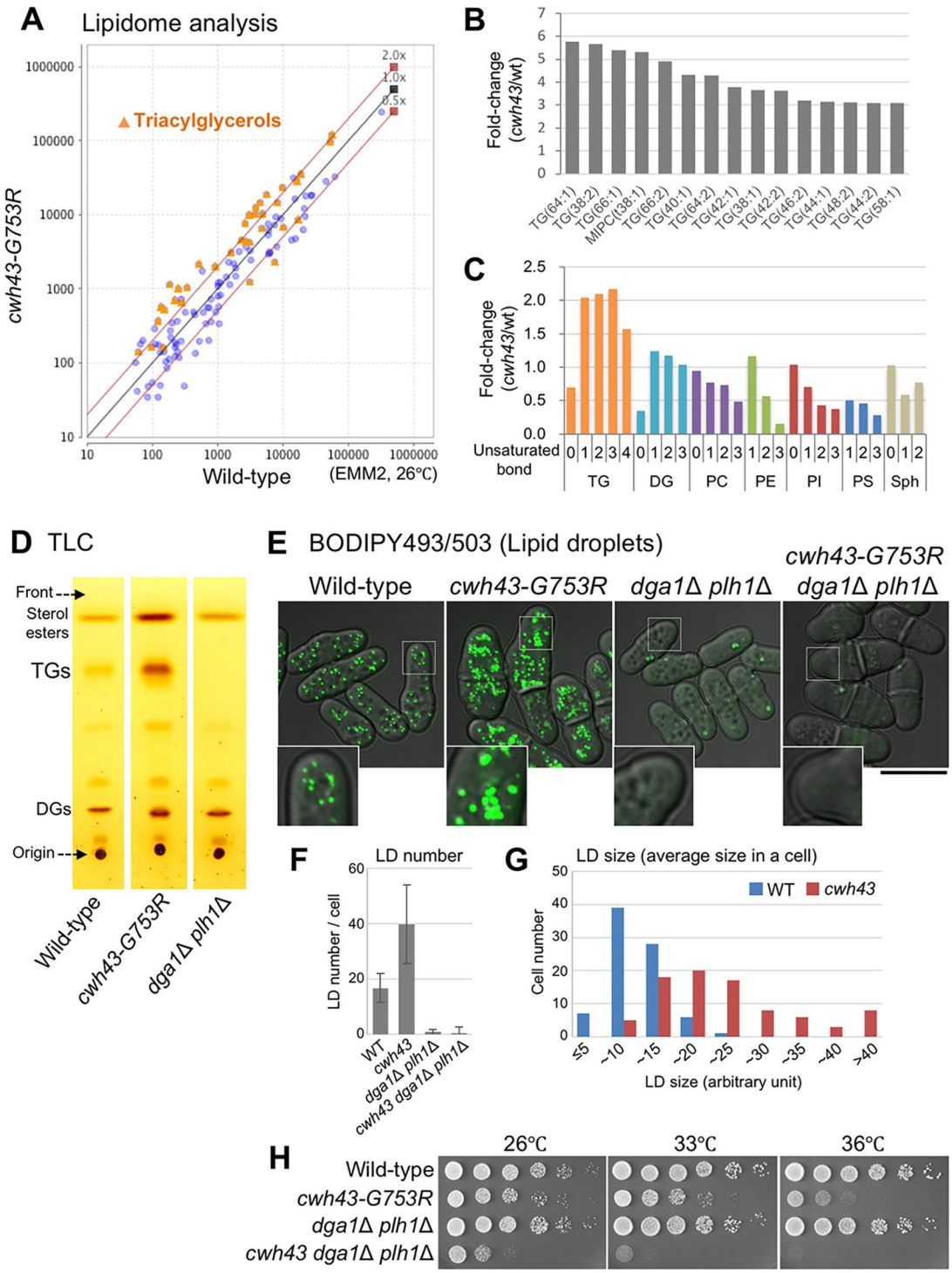

Fig. 6. Increased triacylglycerols and LDs in *cwh43* mutant cells. (A) Lipidomic analysis of cellular extracts in wild-type and *cwh43-G753R* cells. Normalized peak areas of 124 lipid compounds are presented as a scatterplot. Cells were cultivated in EMM2 medium at 26°C and extracted lipid samples were analyzed by LC/MS. Plots for TGs are marked in orange. (B) Levels of 14 TG species increased ∼3–5-fold in mutant cells compared to wild-type cells. MIPC is a complex sphingolipid (mannosylinositol phosphorylceramide). (C) TG species composed of unsaturated fatty acids were increased in *cwh43* mutant cells. The degrees of change (the ratios of *cwh43* to WT) of triacylglycerols (TG), diacylglycerols (DG), phosphatidylcholine (PC), phosphatidylethanolamine (PE), phosphatidylinositol (PI), phosphatidylserine (PS) and phytosphingosine (Sph) are shown with numbers of unsaturated bonds. The sum of detected lipids in *cwh43* mutant was compared with wild-type in each category. (D) The *cwh43-G753R* mutant accumulated TGs while *dga1Δ plh1Δ* double-mutant failed to produce them, as shown via TLC of total lipids. Positions of TGs, DGs and sterol esters are indicated with the origin of sample spot and the solvent front. (E) LDs were stained with the fluorescent dye BODIPY 493/503 in wild-type, *cwh43-G753R*, *dga1Δ plh1Δ* and *cwh43-G753R dga1Δ plh1Δ* mutant strains at 26°C. Dga1 and Plh1 catalyze production of TGs from DGs through distinct reactions (Meyers et al., 2016). Differential interference contrast (DIC) images were merged with fluorescence images. Inserts correspond to the area of the white dashed boxes. Scale bar: 10 µm. (F) Mean±s.d. (n=81, 85, 62 and 67 cells for wild type, *cwh43-G753R, dga1Δ plh1Δ* and *cwh43-G753R dga1Δ plh1Δ* strains, respectively) of the LD number in a cell. (G) Distribution of LD size in wild-type and *cwh43* mutant cells. The mean LD size in each cell is shown in arbitrary units. (H) Severe synthetic growth defect of triple mutants between *cwh43-G753R* and *dga1Δ plh1Δ* double mutants.

Journal of Cell Science (2018) 131, jcs217331. doi:10.1242/jcs.217331

*G753R dga1*Δ *plh1*Δ triple mutant cells also scarcely showed LDs, demonstrating that elevated LD formation in *cwh43* mutant cells requires the TG biosynthesis pathway.

The *dga1*Δ *plh1*Δ double mutant grew normally; however, *cwh43-G753R* and *dga1*Δ *plh1*Δ mutants were additively defective in colony formation at 26–36°C (Fig. 6H). This negative genetic interaction was striking and indicated that LD formation is indispensable for cell division in Cwh43-deficient cells. Since this synthetic phenotype remained in the presence of 1.2 M sorbitol (Fig. S5A), the positive effect of TG synthesis on *cwh43* mutant cells may be independent of morphological recovery. Simultaneous depletion of *dga1*$^{+}$ and *plh1*$^{+}$ genes in *cwh43* mutant apparently abolished sensitivity to glucose limitation, implying that the LGS phenotype of *cwh43* mutant depends on TG synthesis (Fig. S5B).

DISCUSSION

In the present study, we identified multiple ts mutant strains defective in *S. pombe* Cwh43 and characterized their phenotypes. Among the eight ts strains, we identified seven *cwh43* ts mutants that showed sensitivities to both nitrogen starvation and glucose-limited conditions. Identification of these mutant phenotypes is unique in suggesting that Cwh43 contributes to coordinated utilization of distinct major nutrients. Metabolomic analysis indicates that Cwh43-defective cells suffer from nutrient stresses and decline in metabolic activity required for cell division, even in the presence of nutrients. Our results provide the first evidence that Cwh43, which is a proposed ceramide-conjugating protein, strongly affects cellular metabolism of principal nutrients and maintains storage lipid homeostasis.

What is the physiological significance of TG accumulation and its requirement for cell division in *cwh43* mutant cells? First, these results suggest that TGs may function as a critical energy reserve under nutritional stress caused by carbon and nitrogen starvation in cells with defective Cwh43. In fact, wild-type *S. pombe* cells under nitrogen starvation significantly increase the cellular level of TGs accompanying formation of massive LDs (Fig. S6A,B). Consistent with this, both the protein and mRNA levels of two TG synthetic enzymes, Dga1 and Plh1, were upregulated in nitrogen-starved G0 quiescent cells (Fig. S6C,D,E). These levels were not significantly changed between wild-type and the *cwh43* mutant, suggesting that the mechanism of TG accumulation in *cwh43* mutant cells differs from that in wild-type G0 cells.

An alternative possibility for the significance of TG accumulation is that TGs preserve altered plasma membranes in *cwh43* mutant cells. The activity of storage lipid synthesis affects membrane lipid metabolism in budding and fission yeast (Gaspar et al., 2011; He et al., 2014; Péter et al., 2017). Considering that *dga1*Δ *plh1*Δ double mutants grew as well as wild-type cells under normal culture conditions, TG synthesis is deduced to be non-essential for cell growth in the presence of functional Cwh43. In sharp contrast, with impaired Cwh43, TGs may reinforce the disorganized membranes, in which ceramide incorporation is probably defective, compensating for the loss of cell division ability. The increased level of TGs containing unsaturated fatty acids may confer fluidity on the plasma membrane in *cwh43* mutant cells. However, because LDs originate at the ER, where Dga1 and Plh1 proteins localize (Meyers et al., 2016; Thiam et al., 2013), we cannot exclude the possibility that Cwh43 directly affects formation of LDs at the ER.

cwh43 mutant cells are defective in cell division under low glucose and alter the level of metabolic markers for glucose limitation, despite the fact that mutant cells consume glucose from the culture medium. These facts appear inconsistent, but suggest the possibility that *cwh43* mutants may fail to utilize glucose properly after its uptake. Furthermore, we presented genetic evidence that *cwh43* mutant shows sensitivity to glucose limitation only in the presence of *dga1*$^{+}$ and *plh1*$^{+}$ genes (Fig. S5B). Thus, we hypothesize that *cwh43* mutant cells preferentially consume the principal nutrients for TG production. In nutritionally rich media, carbon and nitrogen sources may be converted into TGs for maintaining cell division in *cwh43* mutant; however, TG production may be decreased in mutant cells under nutritionally limiting conditions.

The drastic increase of the iron-storage compounds, ferrichrome and deferriferrichrome, in *cwh43* mutant implies cellular iron deficiency. *S. pombe* has two separate iron uptake pathways. The first is reductive iron transport, employing Frp1 (an Fe^{3+} reductase), Fio1 (an Fe^{2+} oxidase) and Fip1 (an Fe^{3+} permease). The second is non-reductive transport, which acquires ferrichrome-bound iron via the specific transporters Str1, Str2 and Str3. Hence, one possibility is that localization of these iron transporters at the plasma membrane might be adversely affected in *cwh43* mutant cells. Alternatively, we assume that the transcriptional response to iron deficiency may be coupled with glucose limitation. Transcriptional repressors for genes encoding iron transporters and ferrichrome synthetases are actually shared with those of genes involved in the response to low glucose (Janoo et al., 2001; Labbé et al., 2007; Mercier and Labbe, 2010).

We found that a drastically increased CoA level is characteristic of the metabolic phenotype of Cwh43-defective cells. CoA is biosynthesized from pantothenate in five reactions and acts as an acyl carrier involved in numerous metabolic reactions, including fatty acid synthesis (Leonardi et al., 2005; Srinivasan and Sibon, 2014). As an initial reaction, CoA is utilized for production of acetyl-CoA. Therefore, our results raise the possibility that elevated levels of CoA in *cwh43* mutants accelerate acetyl-CoA synthesis. Generally, excessive acetyl-CoA enables fatty acid synthesis and increases triacylglycerol production. In contrast, the *S. pombe ppc1-537* mutant, defective in phosphopantothenoylcysteine synthetase, which catalyzes the second step of CoA synthesis from pantothenate, decreases acetyl-CoA levels and suppresses LD formation (Nakamura et al., 2012). Cwh43 deficiency may thus create a cellular environment in which CoA levels increase to a greater extent than in wild-type cells, promoting triacylglycerol accumulation via acetyl-CoA and fatty acid synthesis. Hydrolysis of thioester bonds in CoA-conjugated metabolites releases high free energy ($\Delta G^{\circ\prime}=-31.4$ kJ/mol), which is comparable to that of ATP hydrolysis ($\Delta G^{\circ\prime}=-30.5$ kJ/mol), implying that *cwh43* mutant cells may consume the cellular energy stored in numerous CoA derivatives and maintain their survival under nutrient stresses. Further study is definitively required to understand metabolic changes implicated in CoA accumulation in Cwh43-deficient cells and its relationship to availability of principal nutrients.

The broad phenotypes in *cwh43* mutant cells can be explained by hypothesizing that Cwh43 properly organizes plasma membranes to provide functional platforms for nutrient signaling and also for cytokinesis. *S. cerevisiae* CWH43 is proposed to be essential for conjugation of ceramide to GPI-anchored proteins (GPI-APs). Indeed, the *S. pombe* Cwh43 C-terminal amino acid sequence around the G753R mutation is highly conserved in both budding and fission yeasts. GPI-APs are modified at the ER and then recruited to the plasma membrane, where they act as receptors, cell adhesion factors or enzymes (Fujita and Jigami, 2008; Kinoshita and Fujita, 2016). Ceramide-enriched micro-domains at the plasma membrane, such as lipid rafts, are believed to be centers for signal

transduction in various biological processes (Lingwood and Simons, 2010). Although further analysis is required, we speculate that metabolic and lipidomic alterations in *S. pombe cwh43-G753R* mutant cells are associated with defects in ceramide conjugation.

MATERIALS AND METHODS

Strains and plasmids

S. pombe strains used in this study were derived from haploid wild-type strains 972 (h^-) and 975 (h^+). A collection of temperature-sensitive (ts) strains made by random mutagenesis was used (Hayashi et al., 2004). Mutation sites and amino acid substitutions in *cwh43* ts mutant strains were determined by whole-genome sequencing (Illumina) and confirmed by Sanger dideoxy sequencing. Genetic linkage between the ts phenotype and mutation sites was verified by tetrad analysis. Strains expressing a C-terminal 3HA (hemagglutinin antigen)- or GFP-tagged Cwh43-WT or -G753R were made by chromosomal integration under the native promoter with the kanamycin-resistance gene. Strains expressing GFP-tagged Dga1 and Plh1 were constructed in the same manner as Cwh43–GFP with the hygromycin-resistance gene. Strains overproducing HA-tagged Cwh43 proteins were constructed by replacing the native promoter with the $nmt1^+$ promoter using the pFA6a-kanMX6-P3nmt1 plasmid (Bähler et al., 1998). The plasmid pRep1 carrying the $nmt1^+$ promoter and the $cwh43^+$ cDNA sequence tagged with HA at its C-terminus was also used for overproduction. Deletion of the $cwh43^+$, $dga1^+$, $plh1^+$, $scs2^+$ and $scs22^+$ genes was performed by replacing the entire genomic locus with the hygromycin or nourseothricin (clonNAT)-resistance genes in a haploid strain. C-terminal mCherry-tagged Cut11 strains were made by chromosomal integration under the native promoter. GFP-tagged Ght5 and Ght8 proteins and deletion of the $ght5^+$ were previously described (Saitoh et al., 2015). The strain expressing mCherry-tagged AHDL, an artificial ER marker, was a gift from Dr Snezhana Oliferenko (King's College London, UK).

Growth conditions

S. pombe cells were cultivated in YPD (rich medium) or EMM2 (minimal medium) with modified glucose concentrations as indicated (Moreno et al., 1991). For nitrogen starvation, cells were first cultivated in EMM2 at 26°C and then transferred to nitrogen-deficient EMM2-N medium at 26°C for 24 h (Sajiki et al., 2009). Cell viability was calculated as a percentage of the number of colonies formed versus the number of plated cells. Liquid-cultured cells were counted using a Multisizer 3 (Beckman Coulter).

Fluorescence microscopy and live-cell analysis

DAPI staining was carried out as previously described (Adachi and Yanagida, 1989). Fluorescent staining of 1,3-β-glucan was performed using Aniline Blue, as previously described (Okada and Ohya, 2016). For lipid droplet staining, 10^7 cells were stained in EMM2 medium containing 100 nM BODIPY 493/503 (Thermo Fisher Scientific, D3922) (Meyers et al., 2016). Procedures for live-cell analysis were carried out using a DeltaVision Elite Microscopy System (GE Healthcare) as described previously (Nakazawa et al., 2016). Oil immersion (60× and 100×; NA 1.4; Olympus) or silicon objective lenses (UPLSAPO 60XS2 and 100XS; NA 1.3 and 1.35; Olympus) were used. For time-lapse imaging, cells were loaded into an ONIX microfluidic perfusion chamber (CellASIC, Hayward, CA) and cultivated with a continuous medium supply. All-in-one microscopes BZ9000 and BZ-X700 (Keyence, Osaka, Japan), were used to observe fixed cells.

Protoplast preparation

S. pombe cells, cultured in 10 ml EMM2 medium at 1×10^7 cells/ml, were collected by centrifugation (1700 ***g*** for 3 min) and washed twice with an equal volume of SCS buffer (20 mM sodium citrate pH 5.8, 1 M sorbitol). Harvested cells were re-suspended in 1 ml SCS containing 2 mg/ml zymolyase 100T (Seikagaku, Tokyo, Japan) and 2 mg/ml lysing enzymes (Sigma, L1412), and incubated for 60 min at 36°C. After cell wall digestion, protoplasts were washed once with SCS buffer.

Immunochemistry

Protein extracts were prepared by cell breakage with trichloroacetic acid (TCA) and glass beads. Cell cultures were harvested by adding a quarter volume of 100% TCA and extracts were prepared in 10% TCA. Precipitated cell extracts were boiled with LDS sample buffer and loaded onto a custom-made 4–12% gradient Bis-Tris gel with MOPS buffer (NuPAGE, Invitrogen). Immunoblotting was performed using antibodies against HA (Roche, catalog number 11 666 606 001, 1:500), GFP (Roche, catalog number 11 814 460 001, 1:500) and PSTAIR (a gift from Dr Yoshitaka Nagahama, National Institute for Basic Biology, Japan, 1:200).

Measurement of glucose consumption

Glucose consumption was measured as previously described (Saitoh et al., 2015). An aliquot of cell culture was obtained and cell pellets were removed by centrifugation. The amount of glucose remaining in the medium was measured using a Glucose HK Assay Kit (Sigma-Aldrich).

RNA extraction and reverse transcription-quantitative PCR

Total RNA from *S. pombe* cells was extracted using a MasterPure yeast RNA purification kit (Epicentre). Purified RNA was reverse-transcribed using a PrimeScript RT reagent kit (TaKaRa) with oligo dT and random primers according to the manufacturer's instructions. The genomic DNA eraser supplied with the above reagent was used to remove contaminated genomic DNA in the RNA sample. cDNA was quantified using real-time PCR (ExiCycler; Bioneer) with a SYBR Premix Ex Taq II solution (TaKaRa). PCR primer sequences are available upon request.

Metabolomic sample preparation

Metabolomic samples were prepared using procedures described previously (Pluskal et al., 2010b). Briefly, cultured cells (40 ml per sample, 5×10^6 cell/ml) were harvested by vacuum filtration and immediately quenched in −40°C methanol. After cells were collected by centrifugation, internal standards (10 nmol of HEPES and PIPES) were added to each sample. Cells were disrupted using a Multi-Beads Shocker (Yasui Kikai, Osaka, Japan) in 50% methanol. Proteins were removed by filtration with an Amicon Ultra 10-kDa cut-off filter (Millipore). Samples were then concentrated by vacuum evaporation and re-suspended in 40 µl of 50% acetonitrile; 1 µl of sample was used for each LC-MS injection.

Lipidomic analysis and thin-layer chromatography

Cultured cells (10 ml per sample, 5×10^6 cell/ml) were harvested and disrupted in 50% methanol as performed in metabolome sample preparation. Two independent *S. pombe* cell cultures were prepared for each strain. For lipid extraction of *S. pombe* cells, non-polar lipids were first extracted with 750 µl *tert*-butyl methyl ether (TBME) (Matyash et al., 2008) and 250 µl of 40 mM NaCl. Second, polar lipids were extracted with 500 µl TBME with water-saturated-1-butanol (3:2) and mixed with non-polar lipid extracts. Samples were then concentrated by vacuum evaporation and re-suspended in 100 µl of the mixed solvent (water-saturated-1-butanol/2-Propanol/H_2O, 1:1:1); 1 µl of sample was used for each LC-MS injection. For thin-layer chromatography, 40 µl of sample were used as described previously (Meyers et al., 2016).

LC-MS analysis

LC-MS data were acquired using a Paradigm MS4 HPLC system (Michrom Bioresources, Auburn, USA) coupled to an LTQ Orbitrap mass spectrometer (Thermo Fisher Scientific), as described previously (Pluskal et al., 2010b). For metabolome analysis, LC separation was performed on a ZIC-pHILIC column (150 mm×2.1 mm, 5 µm particle size, Merck, Darmstadt, Germany). Acetonitrile (A) and 10 mM ammonium carbonate buffer (pH 9.3) (B) were used as the mobile phase, with gradient elution from 80% (A) to 20% (A) in 30 min, at a flow rate of 100 µl/min. Each sample was analyzed twice, once in negative and once in positive ionization mode. Raw LC-MS data were analyzed using MZmine 2 (version 2.21) software. Data analytical procedures and parameters have been described previously (Pluskal et al., 2010a). Compounds were identified using either commercially available standards (STD) or analysis

of MS/MS spectra (MS/MS) (Table S2). Peak areas were normalized by a weighted contribution of the internal standards (PIPES and HEPES) using MZmine 2. For lipidomic analysis, LC separation was performed on a Hypersil Gold C_{18} column (100 mm×2.1 mm, 3 µm particle size, Thermo Fisher Scientific). 60% acetonitrile, 40% water, 10 mM ammonium formate, 0.1% formic acid (A) and 90% isopropanol, 10% acetonitrile, 10 mM ammonium formate and 0.1% formic acid (B) was used as the mobile phase, with gradient elution from 70% (A) to 0% (A) in 20 min followed by isocratic elution for 10 min, at a flow rate of 100 µl/min. The mass spectrometer was operated in full scan mode with a scan range of 200–1200 *m*/*z*. Peak identification by mass search was performed using Lipidomics Gateway (http://www.lipidmaps.org/) and verified using accurate mass, MS/MS fragmentation patterns and retention times (Table S5). We defined the 'relative peak area' ratio as: relative peak area (ppm)=raw peak area/total raw peak area×10^6. Raw LC-MS data in mzML format are accessible via the MetaboLights repository (http://www.ebi.ac.uk/metabolights). Metabolomic and lipidomic analysis data are available under accession numbers MTBLS577 and MTBLS578, respectively.

Acknowledgements
We are indebted to Dr Yukinobu Nakaseko for analyzing the mutation sites of the original *cwh43* ts mutant strains in an initial stage of this work and to Dr Snezhana Oliferenko for providing the mCherry-tagged AHDL strain. We thank Dr Takeshi Hayashi for providing the mCherry-tagged Cut11 strain, Ms Risa Uehara for assistance with glucose consumption assay and Dr Steven D. Aird for editing the manuscript.

Competing interests
The authors declare no competing or financial interests.

Author contributions
Conceptualization: N.N.; Methodology: N.N., T.T., K.S., K.K., A.V., O.A., J.T., S.S.; Software: T.T.; Validation: N.N., S.S.; Formal analysis: N.N., T.T., K.S., K.K., S.S.; Investigation: N.N.; Resources: N.N.; Data curation: N.N., T.T.; Writing - original draft: N.N., M.Y.; Writing - review & editing: N.N., T.T., K.S., S.S., M.Y.; Visualization: N.N.; Supervision: M.Y.; Project administration: N.N., M.Y.

Funding
This study was supported by grants from the Japan Society for the Promotion of Science (KAKENHI grant JP 17K07394 to S.S.) and by the MEXT-Supported Program for the Strategic Research Foundation at Private Universities from the Ministry of Education, Culture, Sports, Science and Technology, Japan (to S.S.). We are also grateful for the generous support of Okinawa Institute of Science and Technology Graduate University.

Data availability
Metabolomic and lipidomic analysis data are available in the MetaboLights repository (https://www.ebi.ac.uk/metabolights/) under accession numbers MTBLS577 and MTBLS578, respectively.

Supplementary information
Supplementary information available online at
http://jcs.biologists.org/lookup/doi/10.1242/jcs.217331.supplemental

References
Adachi, Y. and Yanagida, M. (1989). Higher order chromosome structure is affected by cold-sensitive mutations in a Schizosaccharomyces pombe gene crm1+ which encodes a 115-kD protein preferentially localized in the nucleus and its periphery. *J. Cell Biol.* **108**, 1195-1207.
Bähler, J., Wu, J.-Q., Longtine, M. S., Shah, N. G., McKenzie, A., Steever, A. B., Wach, A., Philippsen, P. and Pringle, J. R. (1998). Heterologous modules for efficient and versatile PCR-based gene targeting in Schizosaccharomyces pombe. *Yeast* **14**, 943-951.
Broek, D., Bartlett, R., Crawford, K. and Nurse, P. (1991). Involvement of p34cdc2 in establishing the dependency of S phase on mitosis. *Nature* **349**, 388-393.
Cansado, J., Vicente-Soler, J., Soto, T., Fernandez, J. and Gacto, M. (1998). Trehalose-6P synthase is essential for trehalase activation triggered by glucose, nitrogen source or heat shock, but not by osmostress, in Schizosaccharomyces pombe. *Biochim. Biophys. Acta* **1381**, 271-278.
Chaurasia, B. and Summers, S. A. (2015). Ceramides–lipotoxic inducers of metabolic disorders. *Trends Endocrinol. Metab.* **26**, 538-550.
Cheah, I. K. and Halliwell, B. (2012). Ergothioneine; antioxidant potential, physiological function and role in disease. *Biochim. Biophys. Acta* **1822**, 784-793.
Chen, R. E. and Thorner, J. (2007). Function and regulation in MAPK signaling pathways: lessons learned from the yeast Saccharomyces cerevisiae. *Biochim. Biophys. Acta* **1773**, 1311-1340.
Cyert, M. S. (2003). Calcineurin signaling in Saccharomyces cerevisiae: how yeast go crazy in response to stress. *Biochem. Biophys. Res. Commun.* **311**, 1143-1150.
Dlakić, M. (2000). Functionally unrelated signalling proteins contain a fold similar to Mg2+-dependent endonucleases. *Trends Biochem. Sci.* **25**, 272-273.
Elbein, A. D., Pan, Y. T., Pastuszak, I. and Carroll, D. (2003). New insights on trehalose: a multifunctional molecule. *Glycobiology* **13**, 17R-27R.
Fujita, M. and Jigami, Y. (2008). Lipid remodeling of GPI-anchored proteins and its function. *Biochim. Biophys. Acta* **1780**, 410-420.
Gaspar, M. L., Hofbauer, H. F., Kohlwein, S. D. and Henry, S. A. (2011). Coordination of storage lipid synthesis and membrane biogenesis. *J. Biol. Chem.* **286**, 1696-1708.
Ghugtyal, V., Vionnet, C., Roubaty, C. and Conzelmann, A. (2007). CWH43 is required for the introduction of ceramides into GPI anchors in Saccharomyces cerevisiae. *Mol. Microbiol.* **65**, 1493-1502.
Hannun, Y. A. (1996). Functions of ceramide in coordinating cellular responses to stress. *Science* **274**, 1855-1859.
Hannun, Y. A. and Obeid, L. M. (2008). Principles of bioactive lipid signalling: lessons from sphingolipids. *Nat. Rev. Mol. Cell Biol.* **9**, 139-150.
Hanyu, Y., Imai, K. K., Kawasaki, Y., Nakamura, T., Nakaseko, Y., Nagao, K., Kokubu, A., Ebe, M., Fujisawa, A., Hayashi, T. et al. (2009). Schizosaccharomyces pombecell division cycle under limited glucose requires Ssp1 kinase, the putative CaMKK, and Sds23, a PP2A-related phosphatase inhibitor. *Genes Cells* **14**, 539-554.
Hayashi, T., Fujita, Y., Iwasaki, O., Adachi, Y., Takahashi, K. and Yanagida, M. (2004). Mis16 and Mis18 are required for CENP-A loading and histone deacetylation at centromeres. *Cell* **118**, 715-729.
He, Y., Yam, C., Pomraning, K., Chin, J. S. R., Yew, J. Y., Freitag, M. and Oliferenko, S. (2014). Increase in cellular triacylglycerol content and emergence of large ER-associated lipid droplets in the absence of CDP-DG synthase function. *Mol. Biol. Cell* **25**, 4083-4095.
Janoo, R. T., Neely, L. A., Braun, B. R., Whitehall, S. K. and Hoffman, C. S. (2001). Transcriptional regulators of the Schizosaccharomyces pombe fbp1 gene include two redundant Tup1p-like corepressors and the CCAAT binding factor activation complex. *Genetics* **157**, 1205-1215.
Kinoshita, T. and Fujita, M. (2016). Biosynthesis of GPI-anchored proteins: special emphasis on GPI lipid remodeling. *J. Lipid Res.* **57**, 6-24.
Krahmer, N., Farese, R. V. and Walther, T. C. (2013). Balancing the fat: lipid droplets and human disease. *EMBO Mol. Med.* **5**, 973-983.
Labbé, S., Pelletier, B. and Mercier, A. (2007). Iron homeostasis in the fission yeast Schizosaccharomyces pombe. *Biometals* **20**, 523-537.
Leonardi, R., Zhang, Y.-M., Rock, C. O. and Jackowski, S. (2005). Coenzyme a: back in action. *Prog. Lipid Res.* **44**, 125-153.
Levin, D. E., Fields, F. O., Kunisawa, R., Bishop, J. M. and Thorner, J. (1990). A candidate protein kinase C gene, PKC1, is required for the S. cerevisiae cell cycle. *Cell* **62**, 213-224.
Lingwood, D. and Simons, K. (2010). Lipid rafts as a membrane-organizing principle. *Science* **327**, 46-50.
Long, A. P., Manneschmidt, A. K., VerBrugge, B., Dortch, M. R., Minkin, S. C., Prater, K. E., Biggerstaff, J. P., Dunlap, J. R. and Dalhaimer, P. (2012). Lipid droplet de novo formation and fission are linked to the cell cycle in fission yeast. *Traffic* **13**, 705-714.
Martin-Yken, H., Dagkessamanskaia, A., De Groot, P., Ram, A., Klis, F. and Francois, J. (2001). Saccharomyces cerevisiae YCRO17c/CWH43encodes a putative sensor/transporter protein upstream of the BCK2branch of the PKC1-dependent cell wall integrity pathway. *Yeast* **18**, 827-840.
Matyash, V., Liebisch, G., Kurzchalia, T. V., Shevchenko, A. and Schwudke, D. (2008). Lipid extraction by methyl- tert-butyl ether for high-throughput lipidomics. *J. Lipid Res.* **49**, 1137-1146.
Mercier, A. and Labbe, S. (2010). Iron-dependent remodeling of fungal metabolic pathways associated with ferrichrome biosynthesis. *Appl. Environ. Microbiol.* **76**, 3806-3817.
Meyers, A., del Rio, Z. P., Beaver, R. A., Morris, R. M., Weiskittel, T. M., Alshibli, A. K., Mannik, J., Morrell-Falvey, J. and Dalhaimer, P. (2016). Lipid droplets form from distinct regions of the cell in the fission yeast Schizosaccharomyces pombe. *Traffic* **17**, 657-669.
Meyers, A., Weiskittel, T. M. and Dalhaimer, P. (2017). Lipid droplets: formation to breakdown. *Lipids* **52**, 465-475.
Moreno, S., Klar, A. and Nurse, P. (1991). Molecular genetic analysis of fission yeast Schizosaccharomyces pombe. *Meth. Enzymol.* **194**, 795-823.
Nakamura, T., Pluskal, T., Nakaseko, Y. and Yanagida, M. (2012). Impaired coenzyme A synthesis in fission yeast causes defective mitosis, quiescence-exit failure, histone hypoacetylation and fragile DNA. *Open Biol.* **2**, 120117-120117.
Nakazawa, N., Mehrotra, R., Arakawa, O. and Yanagida, M. (2016). ICRF-193, an anticancer topoisomerase II inhibitor, induces arched telophase spindles that snap, leading to a ploidy increase in fission yeast. *Genes Cells* **21**, 978-993.

Oelkers, P., Tinkelenberg, A., Erdeniz, N., Cromley, D., Billheimer, J. T. and Sturley, S. L. (2000). A lecithin cholesterol acyltransferase-like gene mediates diacylglycerol esterification in yeast. *J. Biol. Chem.* **275**, 15609-15612.
Oelkers, P., Cromley, D., Padamsee, M., Billheimer, J. T. and Sturley, S. L. (2002). The DGA1Gene determines a second triglyceride synthetic pathway in yeast. *J. Biol. Chem.* **277**, 8877-8881.
Okada, H. and Ohya, Y. (2016). Fluorescent labeling of yeast cell wall components. *Cold Spring Harb. Protoc.* **2016**, pdb.prot085241–5.
Perez, P. and Cansado, J. (2010). Cell integrity signaling and response to stress in fission yeast. *Curr. Protein Pept Sci.* **11**, 680-692.
Péter, M., Glatz, A., Gudmann, P., Gombos, I., Török, Z., Horváth, I., Vígh, L. and Balogh, G. (2017). Metabolic crosstalk between membrane and storage lipids facilitates heat stress management in Schizosaccharomyces pombe. *PLoS ONE* **12**, e0173739.
Pidoux, A. L. and Armstrong, J. (1993). The BiP protein and the endoplasmic reticulum of Schizosaccharomyces pombe: fate of the nuclear envelope during cell division. *J. Cell Sci.* **105**, 1115-1120.
Pluskal, T., Castillo, S., Villar-Briones, A. and Orešič, M. (2010a). MZmine 2: modular framework for processing, visualizing, and analyzing mass spectrometry-based molecular profile data. *BMC Bioinformatics* **11**, 395.
Pluskal, T., Nakamura, T., Villar-Briones, A. and Yanagida, M. (2010b). Metabolic profiling of the fission yeast S. pombe: quantification of compounds under different temperatures and genetic perturbation. *Mol. BioSyst.* **6**, 182-198.
Pluskal, T., Hayashi, T., Saitoh, S., Fujisawa, A. and Yanagida, M. (2011). Specific biomarkers for stochastic division patterns and starvation-induced quiescence under limited glucose levels in fission yeast. *FEBS J.* **278**, 1299-1315.
Pol, A., Gross, S. P. and Parton, R. G. (2014). Review: biogenesis of the multifunctional lipid droplet: lipids, proteins, and sites. *J. Cell Biol.* **204**, 635-646.
Reggiori, F., Canivenc-Gansel, E. and Conzelmann, A. (1997). Lipid remodeling leads to the introduction and exchange of defined ceramides on GPI proteins in the ER and Golgi of Saccharomyces cerevisiae. *EMBO J.* **16**, 3506-3518.
Saitoh, S., Mori, A., Uehara, L., Masuda, F., Soejima, S. and Yanagida, M. (2015). Mechanisms of expression and translocation of major fission yeast glucose transporters regulated by CaMKK/phosphatases, nuclear shuttling, and TOR. *Mol. Biol. Cell* **26**, 373-386.
Sajiki, K., Hatanaka, M., Nakamura, T., Takeda, K., Shimanuki, M., Yoshida, T., Hanyu, Y., Hayashi, T., Nakaseko, Y. and Yanagida, M. (2009). Genetic control of cellular quiescence in S. pombe. *J. Cell Sci.* **122**, 1418-1429.
Sajiki, K., Pluskal, T., Shimanuki, M. and Yanagida, M. (2013). Metabolomic analysis of fission yeast at the onset of nitrogen starvation. *Metabolites* **3**, 1118-1129.
Schrettl, M., Winkelmann, G. and Haas, H. (2004). Ferrichrome in Schizosaccharomyces pombe–an iron transport and iron storage compound. *Biometals* **17**, 647-654.
Shiozaki, K. and Russell, P. (1995). Counteractive roles of protein phosphatase 2C (PP2C) and a MAP kinase kinase homolog in the osmoregulation of fission yeast. *EMBO J.* **14**, 492-502.
Shirai, A., Matsuyama, A., Yashiroda, Y., Hashimoto, A., Kawamura, Y., Arai, R., Komatsu, Y., Horinouchi, S. and Yoshida, M. (2008). Global analysis of gel mobility of proteins and its use in target identification. *J. Biol. Chem.* **283**, 10745-10752.
Srinivasan, B. and Sibon, O. C. M. (2014). Coenzyme A, more than “just” a metabolic cofactor. *Biochm. Soc. Trans.* **42**, 1075-1079.
Su, S. S., Tanaka, Y., Samejima, I., Tanaka, K. and Yanagida, M. (1996). A nitrogen starvation-induced dormant G0 state in fission yeast: the establishment from uncommitted G1 state and its delay for return to proliferation. *J. Cell Sci.* **109**, 1347-1357.
Sugiura, R., Sio, S. O., Shuntoh, H. and Kuno, T. (2002). Calcineurin phosphatase in signal transduction: lessons from fission yeast. *Genes Cells* **7**, 619-627.
Sugiura, R., Toda, T., Shuntoh, H., Yanagida, M. and Kuno, T. (1998). pmp1+, a suppressor of calcineurin deficiency, encodes a novel MAP kinase phosphatase in fission yeast. *EMBO J.* **17**, 140-148.
Sugiura, R., Toda, T., Dhut, S., Shuntoh, H., Kuno, T. and Kuno, T. (1999). The MAPK kinase Pek1 acts as a phosphorylation-dependent molecular switch. *Nature* **399**, 479-483.
Takeda, K., Yoshida, T., Kikuchi, S., Nagao, K., Kokubu, A., Pluskal, T., Villar-Briones, A., Nakamura, T. and Yanagida, M. (2010). Synergistic roles of the proteasome and autophagy for mitochondrial maintenance and chronological lifespan in fission yeast. *Proc. Natl Acad. Sci. USA* **107**, 3540-3545.
Thiam, A. R., Farese, R. V. and Walther, T. C. (2013). The biophysics and cell biology of lipid droplets. *Nature Publishing Group* **14**, 775-786.
Toda, T., Shimanuki, M. and Yanagida, M. (1993). Two novel protein kinase C-related genes of fission yeast are essential for cell viability and implicated in cell shape control. *EMBO J.* **12**, 1987-1995.
Umemura, M., Fujita, M., Yoko-o, T., Fukamizu, A. and Jigami, Y. (2007). Saccharomyces cerevisiae CWH43 is involved in the remodeling of the lipid moiety of GPI anchors to ceramides. *Mol. Biol. Cell* **18**, 4304-4316.
West, R. R., Vaisberg, E. V., Ding, R., Nurse, P. and McIntosh, J. R. (1998). cut11(+): a gene required for cell cycle-dependent spindle pole body anchoring in the nuclear envelope and bipolar spindle formation in Schizosaccharomyces pombe. *Mol. Biol. Cell* **9**, 2839-2855.
Yanagida, M. (2009). Cellular quiescence: are controlling genes conserved? *Trends Cell Biol.* **19**, 705-715.
Yoko-o, T., Ichikawa, D., Miyagishi, Y., Kato, A., Umemura, M., Takase, K., Ra, M., Ikeda, K., Taguchi, R. and Jigami, Y. (2013). Determination and physiological roles of the glycosylphosphatidylinositol lipid remodelling pathway in yeast. *Mol. Microbiol.* **88**, 140-155.
Yoshida, T., Toda, T. and Yanagida, M. (1994). A calcineurin-like gene ppb1+ in fission yeast: mutant defects in cytokinesis, cell polarity, mating and spindle pole body positioning. *J. Cell Sci.* **107**, 1725-1735.
Zhang, Q., Chieu, H. K., Low, C. P., Zhang, S., Heng, C. K. and Yang, H. (2003). Schizosaccharomyces pombe cells deficient in triacylglycerols synthesis undergo apoptosis upon entry into the stationary phase. *J. Biol. Chem.* **278**, 47145-47155.
Zhang, D., Vjestica, A. and Oliferenko, S. (2010). The cortical ER network limits the permissive zone for actomyosin ring assembly. *Curr. Biol.* **20**, 1029-1034.
Zhang, D., Vjestica, A. and Oliferenko, S. (2012). Plasma membrane tethering of the cortical ER necessitates its finely reticulated architecture. *Curr. Biol.* **22**, 2048-2052.

Supplemental Fig. S1

Alignment of Cwh43 amino acid sequences and mutation sites of *S. pombe cwh43* ts mutants identified in this study

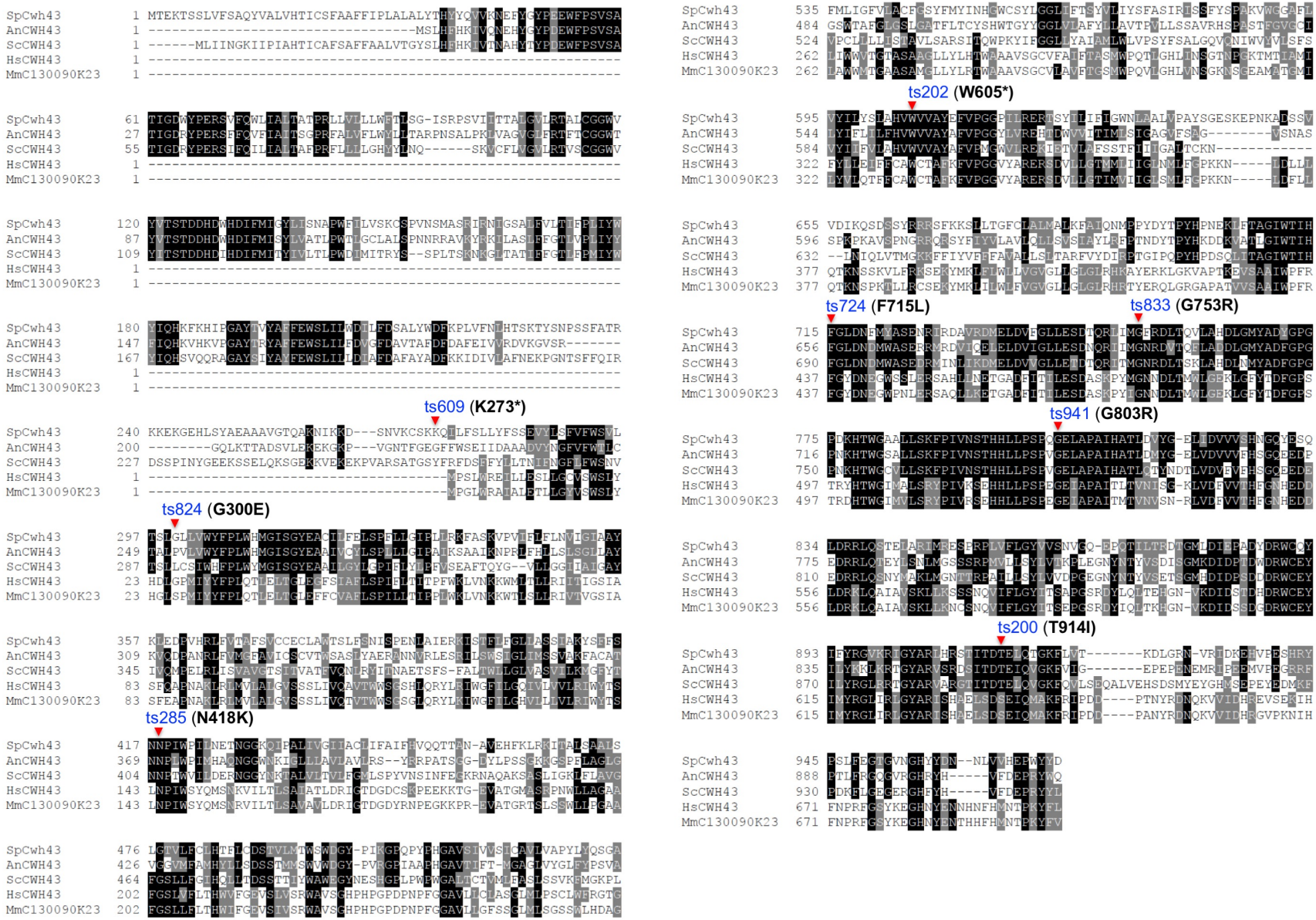

Supplemental Figure S1

Alignment of Cwh43 amino acid sequences and mutation sites of *S. pombe cwh43* ts mutants identified in this study

Aligned amino acid sequences of Cwh43 orthologs in *Schizosaccharomyces pombe* (SpCwh43), *Aspergillus niger* (AnCWH43), *Saccharomyces cerevisiae* (ScCWH43), *Homo sapiens* (HsCWH43), and *Mus musculus* (MmC130090K23). Human CWH43/FLJ21511 and mouse C130090K23 proteins homologous to the C-terminus of yeast Cwh43 are aligned. Mutation sites of *S. pombe cwh43* ts mutants identified in this study are indicated.

Supplemental Fig. S2

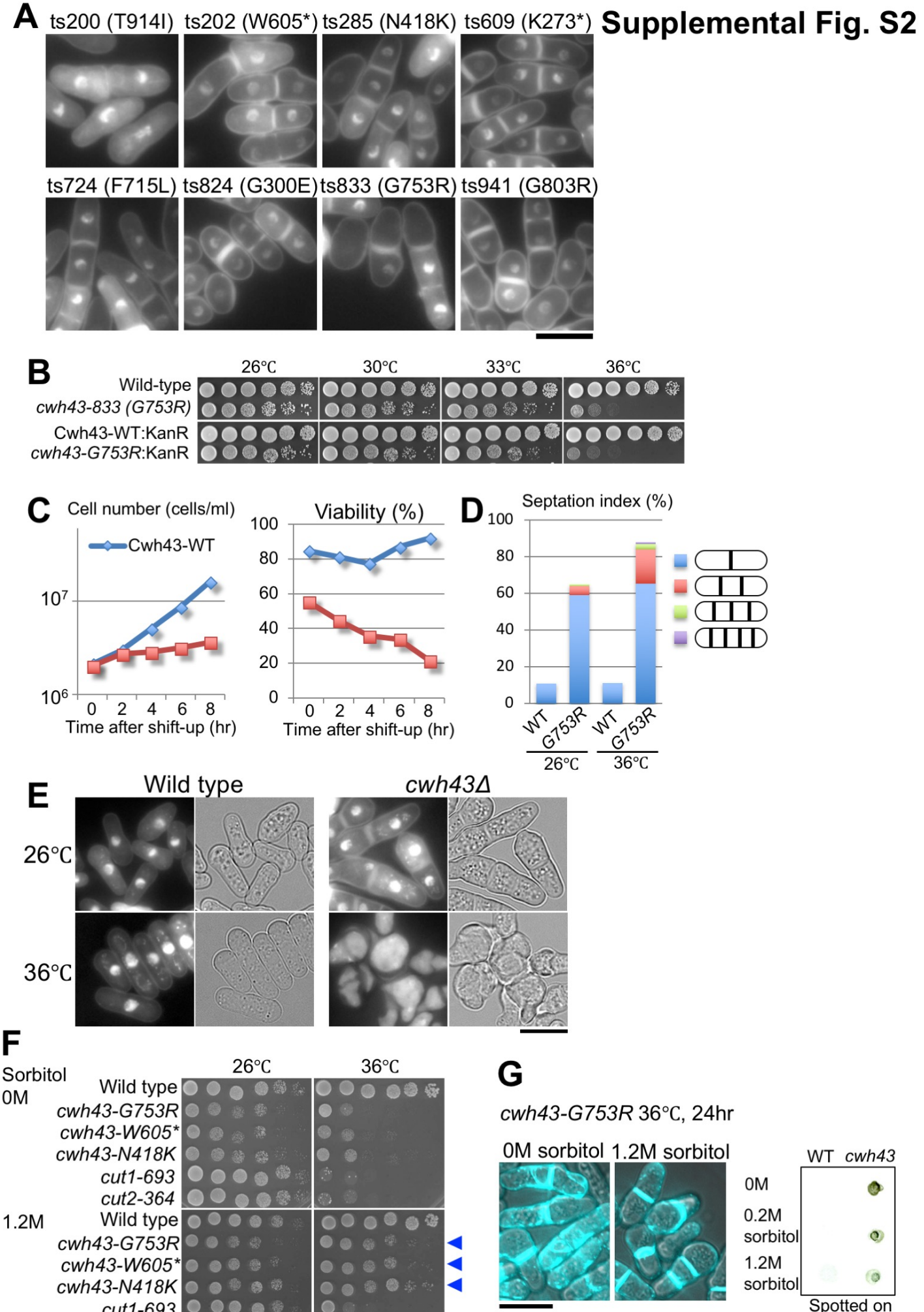

Supplemental Figure S2

Morphological phenotypes in 8 *cwh43* ts mutants and *cwh43*Δ deletion mutant cells

(A) Wild-type and 8 *cwh43* ts mutant strains (ts200, ts202, ts285, ts609, ts724, ts824, ts833, ts941) were cultured at 26°C and shifted to 36°C for 5 hr, and stained with DAPI. Amino acid changes of 8 *cwh43* ts mutant strains are shown in parentheses. Asterisks indicate stop codons. Bar, 10 μm. **(B)** Strains expressing chromosomally-integrated, HA-tagged Cwh43-WT:KanR (kanamycin resistant) or -*G753R*:KanR genes were spotted on YPD solid media along with non-tagged wild-type and original *cwh43-833* mutant strains. **(C)** Wild-type and *cwh43-G753R* strains were cultivated at 26°C, and then shifted to 36°C for 8 hr to measure cell number (left) and viability (right). **(D)** Proportions of cells with single or multiple septa (septation index) are shown. **(E)** DAPI-stained and bright field micrographs of *cwh43*Δ deletion mutant cells at 26°C or 36°C for 6 hr. Bar, 10 μm. **(F)** Suppression of ts phenotypes in multiple *cwh43* mutants by sorbitol treatment. Arrowheads indicate ts suppression in *cwh43-G753R*, *-W605**, and *-N418K* mutant strains. Ts of *cut1-693* and *cut2-364* mutants were also suppressed by sorbitol as reported previously (Kawasaki et al., 2006). **(G)** Abnormal accumulation of 1, 3-β-glucan was partly alleviated by sorbitol treatment. (Left) Fluorescent and bright field images of *cwh43-G753R* cells were captured after staining for the cell wall component, 1, 3-β-glucan, using the fluorescent dye, aniline blue. Cells were cultured at 36°C for 24 hr in liquid media in the presence or absence of 1.2 M sorbitol. Scale bar, 10 μm. (Right) Aniline blue-stained cells were spotted on filter paper.

Supplemental Fig. S3

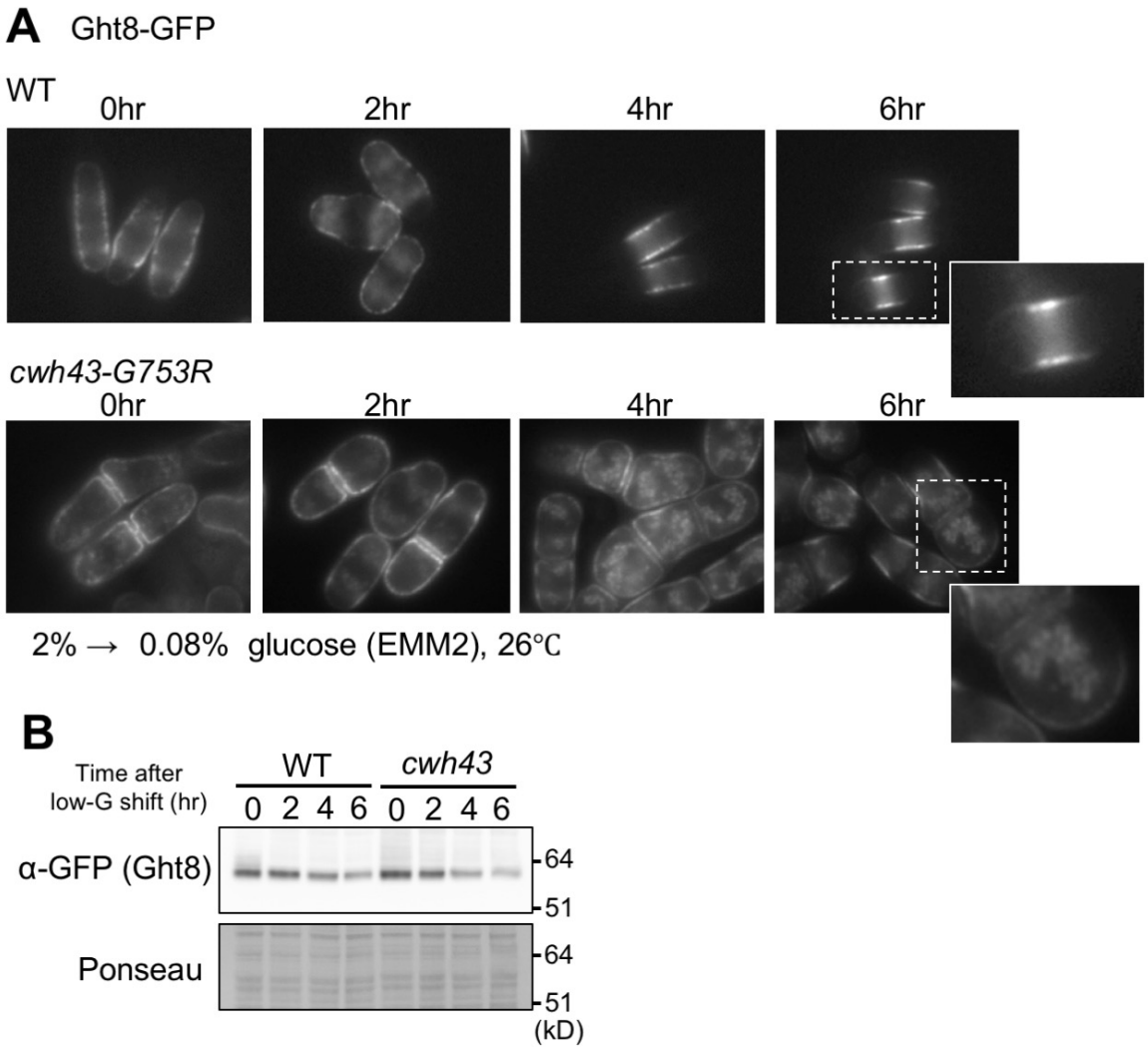

Supplemental Figure S3

Localization of the GFP-tagged hexose transporter, Ght8, at the cell surface is altered in *cwh43-G753R* mutant cells

(A) Expression and localization of GFP-tagged Ght8 proteins in wild-type (top) and *cwh43-G753R* (bottom) mutant cells are shown. Cells were cultivated in EMM2 liquid media at 26°C and the glucose concentration was switched from 2% (111 mM) to 0.08% (4.4 mM) at time 0 hr. GFP fluorescence microscopic images were taken at 2-hr intervals. Inserts correspond to the white dashed boxes. Scale bar, 10 μm. **(B)** The protein level of Ght8-GFP was measured by immunoblot. Total proteins stained with Ponceau S is shown as a loading control.

Supplemental Fig. S4

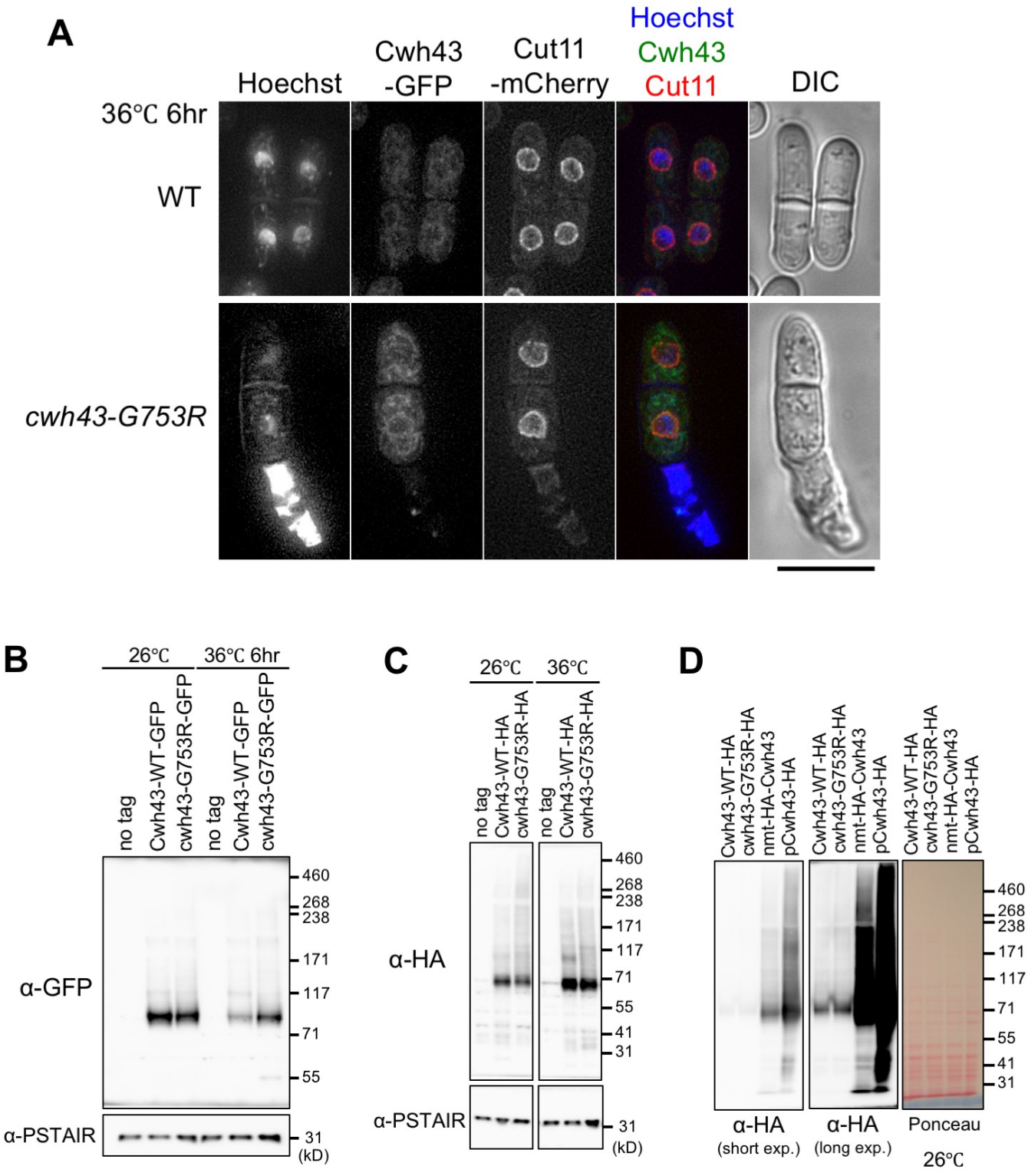

Supplemental Figure S4

Localization of GFP-tagged Cwh43 protein at 36°C, and detection of endogenous and overproduced Cwh43 proteins in SDS-PAGE

(A) Intracellular localization of GFP-tagged Cwh43-WT and -G753R proteins at 36°C. Cells were cultivated at 36°C for 6 hr in EMM2 media and fluorescent images were captured immediately without fixation, as shown in Fig. 4A. A single focal plane is shown. Scale bar, 10 μm. (**B, C**) Cells expressing chromosomally-integrated, and GFP- (B) or HA- (C)-tagged Cwh43-WT and -G753R proteins under the native promoter were cultured at 26°C and then shifted to 36°C for 6 hr, along with untagged wild-type strain. Protein extracts were then prepared and immunoblotted with anti-GFP or anti-HA antibody. The anti-PSTAIR antibody against Cdc2 was used as a loading control. An immunoblot of Cwh43-GFP at 26°C, presented in Fig. 4D, is shown in (B) for comparison. (**D**) Cwh43-WT-HA and -G753R-HA proteins were immunoblotted with anti-HA antibody, along with blotting for overexpressed HA-fused Cwh43-WT proteins derived from chromosomally-integrated single-copy (nmt-HA-Cwh43) or plasmid-borne multi-copy (pCwh43-HA) genes under the nmt promoter. Short (left) and long (middle) exposed images of the immunoblot are shown. The pattern of total proteins stained with Ponceau S is also shown as a loading control (right).

Supplemental Fig. S5

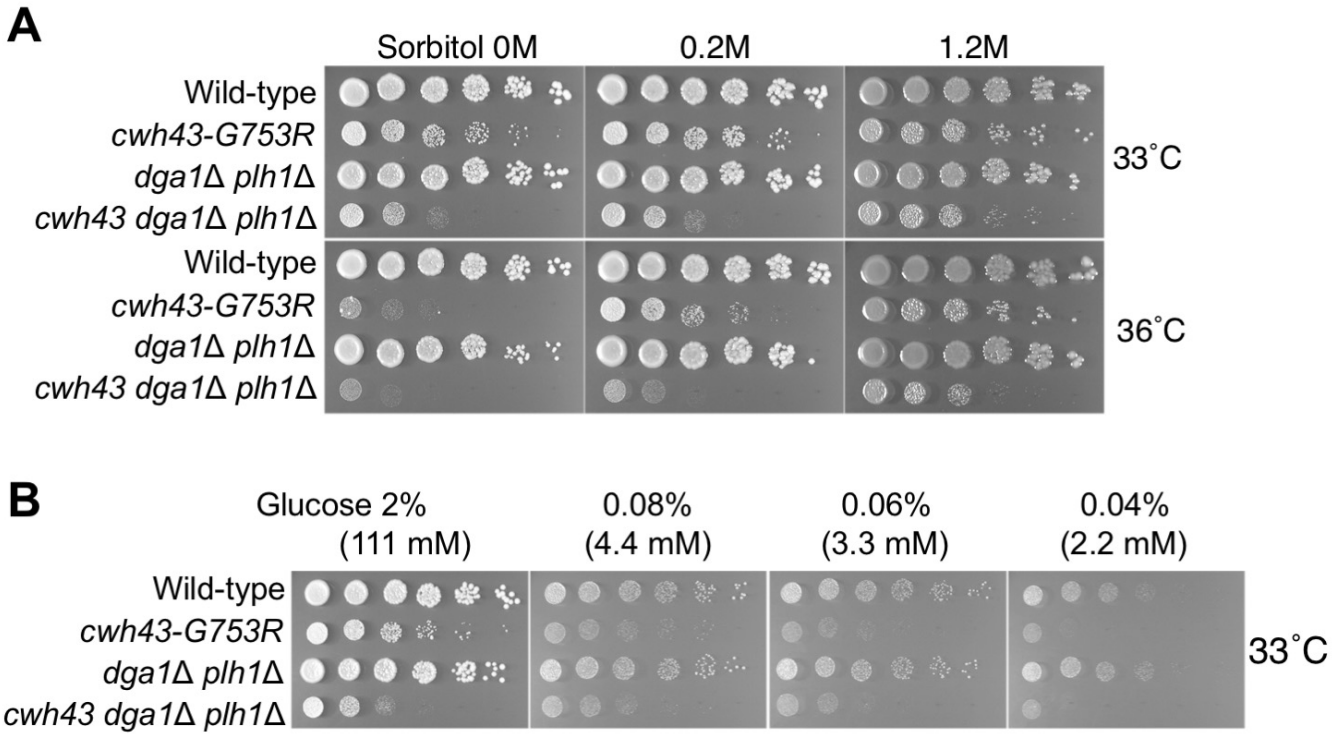

Supplemental Figure S5

Effects of sorbitol addition and glucose limitation on the *cwh43-G753R dga1Δ plh1Δ* triple mutant

(A) Synthetic growth defect between the *cwh43-G753R* mutant and the *dga1Δ plh1Δ* double mutant remained in the presence of sorbitol. **(B)** *dga1Δ plh1Δ* double deletion apparently abolished the sensitivity to glucose limitation in *cwh43-G753R* mutant. Aliquots ($5x10^4$ cells) of cells were serially diluted 5x, spotted onto EMM2 media containing the indicated concentrations (mM and percentage) of glucose at 33°C.

Supplemental Fig. S6

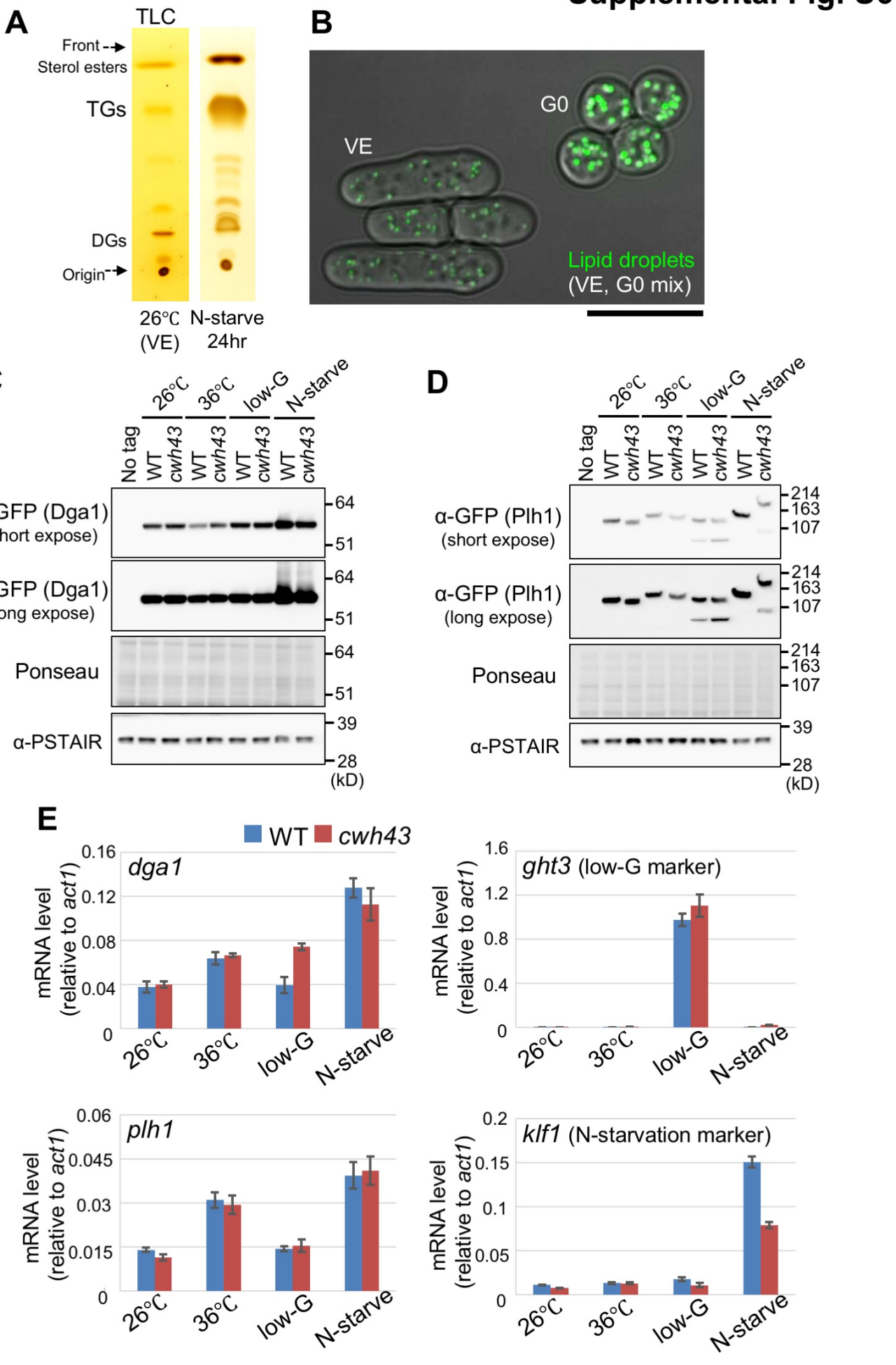

Supplemental Figure S6

Protein and mRNA levels of two TG synthetic enzymes, Dga1 and Plh1, are not significantly changed between wild-type and *cwh43* mutant cells

(A) *S. pombe* wild-type cells under nitrogen starvation accumulate TGs. Thin-layer chromatography (TLC) of total lipids showed *S. pombe* wild-type cells accumulated TGs in nitrogen-starved G0 quiescent cells. Positions of TGs, DGs (diacylglycerols), and sterol esters are indicated with the origin of sample spot and the solvent front. **(B)** Cultivated wild-type vegetative and G0 cells were mixed at 26°C, and lipid droplets (LDs) were stained with the fluorescent dye BODIPY 493/503. Differential interference contrast (DIC) images were merged with fluorescent images. Scale bar, 10 μm. **(C, D)** Protein levels of Dga1 (C) and Plh1 (D) were measured by immunoblot in wild-type and *cwh43-G753R* mutant cells. Cells expressing GFP-tagged Dga1 or Plh1 proteins under the native promoter were constructed by chromosomal integration at endogenous loci in wild-type and *cwh43* mutant. These cells were cultured at 26°C and then shifted to the following four conditions; (1) 26°C for 6 hr, (2) 36°C for 6 hr, (3) 0.08% glucose at 26°C for 6 hr (low-G), (4) nitrogen starvation at 26°C for 24 hr (N-starve), along with untagged wild-type cells. Protein extracts were then prepared and immunoblotted with anti-GFP antibody. The anti-PSTAIR antibody against Cdc2 and Ponceau S staining were used as loading control. GFP-tagged Plh1 proteins at 36°C or under nitrogen starvation migrated faster than those in other culture conditions for an unknown reason, especially in *cwh43* mutant cells under nitrogen starvation. **(E)** The mRNA levels of *dga1* and *plh1* were examined in wild-type and *cwh43* mutant cells. Cells were cultivated as indicated in (A), and total RNA samples were obtained. The mRNA levels of $dga1^{+}$ and $plh1^{+}$ genes relative to that of $act1^{+}$ were measured by RT-qPCR, along with $ght3^{+}$ and $klf1^{+}$ genes, as control for low-glucose and nitrogen-starved conditions, respectively (Saitoh et al., 2015; Shimanuki et al., 2013). The mRNA levels were quantified with error bars showing the standard deviation (n = 3).

Supplemental Table S1

Sensitivity to low glucose and viability under nitrogen starvation in 8 *cwh43* ts mutant strains

Strain	Mutation site	Degree of LGS*	Viability under N-starvation (%)		
			Vegetative	-N 24hr at 26℃	additional 3 days at 37℃
Wild-type	-	non-LGS	93	81	74
ts200	T914I	0.02-0.03%	66	55	1
ts202	W605stop	0.02-0.03%	67	55	11
ts285	N418K	0.04-0.06%	68	63	0
ts609	K273stop	0.02-0.03%	67	38	0
ts724	F715L	0.04-0.06%	80	52	13
ts824	G300E	non-LGS	92	52	0
ts833	G753R	0.04-0.06%	61	27	0
ts941	G803R	0.02-0.03%	65	36	39

*Glucose concentration in which mutant strain showed LGS (Low glucose sensitivity)

Supplemental Table S2

Peak list of identified metabolites in wild-type and *cwh43-G753R* mutant cells

Click here to Download Table S2

Supplemental Table S3

Abundance of metabolites in the *cwh43-G753R* mutant (increased more than 3x relative to wild-type cells; normalized peak area)

Rank	Compound	**VE *cwh43*/WT ratio**	VE Wild type	VE *cwh43*
1	Deferriferrichrome	**18941.33**	0.001	22.2
2	CoA	**4547.60**	0.003	14.3
3	2-Oxoglutarate	**88.82**	0.1	11.9
4	Trehalose	**61.41**	13.8	845.6
5	Ergothioneine	**36.06**	0.2	6.4
6	Trehalose-6-phosphate	**25.31**	2.2	54.9
7	Trimethyl-histidine (hercynine)	**12.25**	2.8	33.9
8	Hercynylcysteine sulfoxide	**6.90**	0.06	0.4
9	Ferrichrome	**6.29**	33.6	211.3
10	Adenosine	**6.10**	2.8	16.8
11	HMG-CoA	**5.93**	0.7	4.3
12	Succinate	**5.66**	4.4	24.8
13	Acetyl-CoA	**5.17**	2.9	15.0
14	Inosine	**4.40**	9.8	43.2
15	Proline	**4.29**	0.7	2.9
16	Histidinol	**4.08**	1.3	5.5
17	myo-Inositol	**4.06**	4.4	17.7
18	Asparagine	**3.78**	1.9	7.3
19	Dimethyl-histidine	**3.66**	8.1	29.7
20	UDP-N-acetylglucosamine	**3.53**	25.0	88.3
21	Isoleucine	**3.17**	2.4	7.7
22	1-Methyladenosine	**3.13**	11.8	37.0
23	Glutamine	**3.09**	18.1	55.8
24	Trimethyl-lysine	**3.08**	1.2	3.6
25	N2-Acetyl-lysine	**3.00**	2.1	6.4

Supplemental Table S4

Abundance of metabolites in *cwh43-G753R* mutants (decreased more than 3x relative to wild-type cells; normalized peak area)

Rank	Compound	**VE *cwh43*/WT ratio**	VE Wild type	VE *cwh43*
1	PRPP	**0.02**	12.3	0.3
2	Diphosphoglycerate	**0.02**	1.4	0.03
3	AICAR	**0.09**	4.2	0.4
4	Biotin	**0.11**	9.6	1.0
5	S-Adenosyl-cysteine	**0.12**	3.2	0.4
6	Glutamate methyl ester	**0.18**	3.3	0.6
7	SAICAR	**0.20**	4.2	0.8
8	Cytidine	**0.25**	36.0	9.0
9	S-Adenosyl-homocysteine	**0.30**	47.7	14.4
10	CDP	**0.33**	2.5	0.8

Supplemental Table S5

Peak list of identified lipids in wild-type and *cwh43-G753R* mutant cells

Click here to Download Table S5

Supplemental Table S6

Comparative data for abundance of lipids between wild-type and *cwh43-G753R* mutant cells

Identified peak list

Compounds	relative peak area (ppm)		ratio
	WT	G753R	
Triacylglycerides [47]			
TG(34:0)	61	136	2.23
TG(36:0)	235	685	2.91
TG(36:1)	274	652	2.38
TG(38:0)	123	356	2.90
TG(38:1)	271	987	3.65
TG(38:2)	195	1101	5.65
TG(40:1)	128	552	4.32
TG(42:0)	359	1029	2.87
TG(42:1)	549	2080	3.79
TG(42:2)	139	506	3.64
TG(44:0)	2313	4522	1.95
TG(44:1)	3097	9757	3.15
TG(44:2)	3932	12195	3.10
TG(44:3)	101	161	1.60
TG(46:0)	4842	6770	1.40
TG(46:1)	9934	22848	2.30
TG(46:2)	5711	18260	3.20
TG(48:0)	3058	1289	0.42
TG(48:1)	4938	10171	2.06
TG(48:2)	4540	14196	3.13
TG(50:0)	7455	2314	0.31
TG(50:1)	3078	4088	1.33
TG(50:2)	2711	7526	2.78
TG(52:0)	16737	8292	0.50
TG(52:1)	8277	14773	1.78
TG(52:2)	18911	33890	1.79
TG(52:3)	3855	10205	2.65
TG(52:4)	146	162	1.11
TG(54:0)	10058	6902	0.69
TG(54:1)	15775	27935	1.77
TG(54:2)	53504	98982	1.85
TG(54:3)	56579	115472	2.04
TG(54:4)	2765	4275	1.55
TG(56:1)	898	2297	2.56
TG(56:2)	1636	3131	1.91
TG(58:0)	99	135	1.37
TG(58:1)	1402	4319	3.08
TG(58:2)	1892	3687	1.95
TG(58:3)	584	555	0.95
TG(60:1)	3349	8393	2.51
TG(60:2)	8723	18178	2.08
TG(60:3)	2766	2638	0.95

Compounds	relative peak area (ppm)		ratio
	WT	G753R	
TG(62:2)	349	958	2.74
TG(64:1)	83	475	5.76
TG(64:2)	163	703	4.31
TG(66:1)	84	453	5.39
TG(66:2)	104	512	4.92
Diacylglycerides [14]			
DG(26:0)	190	215	1.13
DG(28:0)	1401	1425	1.02
DG(28:1)	704	548	0.78
DG(30:0)	793	702	0.89
DG(30:1)	1139	1197	1.05
DG(32:1)	241	352	1.46
DG(34:0)	14799	4430	0.30
DG(34:1)	1762	2056	1.17
DG(34:2)	427	466	1.09
DG(36:0)	19796	5779	0.29
DG(36:1)	1482	2199	1.48
DG(36:2)	7603	8767	1.15
DG(36:3)	136	134	0.99
DG(38:2)	89	33	0.38
Phospholipids [52]			
LPC(16:0)	284	706	2.49
LPC(18:0)	117	166	1.41
LPC(18:1)	9156	8489	0.93
PC(24:0)	1099	791	0.72
PC(26:0)	22069	17149	0.78
PC(26:1)	6302	2882	0.46
PC(28:0)	15303	15692	1.03
PC(28:1)	62196	31388	0.50
PC(28:2)	730	197	0.27
PC(30:0)	2161	3053	1.41
PC(30:1)	45964	26891	0.59
PC(30:2)	469	131	0.28
PC(32:0)	144	139	0.97
PC(32:1)	7453	6961	0.93
PC(32:2)	713	339	0.48
PC(34:1)	14633	29995	2.05
PC(34:2)	21159	11584	0.55
PC(36:1)	5908	6866	1.16
PC(36:2)	323604	232910	0.72
PC(36:3)	6019	2830	0.47
PC(38:2)	1041	1056	1.01
LPE(18:1)	222	162	0.73

Compounds	relative peak area (ppm)		ratio
	WT	G753R	
PE(28:1)	162	102	0.63
PE(30:1)	174	111	0.64
PE(32:1)	228	187	0.82
PE(34:1)	5835	5038	0.86
PE(34:2)	3238	2326	0.72
PE(36:1)	324	456	1.41
PE(36:2)	26618	17180	0.65
PE(38:2)	13511	4383	0.32
PE(38:3)	344	48	0.14
LPI(16:0)	56	38	0.69
LPI(18:1)	243	105	0.43
PI(26:0)	970	1104	1.14
PI(28:0)	1837	1733	0.94
PI(28:1)	722	503	0.70
PI(30:0)	434	409	0.94
PI(30:1)	593	445	0.75
PI(32:1)	1469	1049	0.71
PI(34:1)	26261	17111	0.65
PI(34:2)	903	445	0.49
PI(36:1)	2991	2996	1.00
PI(36:2)	21207	8783	0.41
PI(36:3)	506	181	0.36
PS(32:1)	158	78	0.49
PS(34:1)	5924	2871	0.48
PS(34:2)	124	46	0.37
PS(36:1)	265	185	0.70
PS(36:2)	7704	3439	0.45
PS(36:3)	115	31	0.27
PA(34:1)	74	44	0.60
PA(36:2)	96	48	0.50
Sphingolipids [9]			
Sph(t16:1)	1055	332	0.31
Sph(t20:0)	196	274	1.40
Cer(d38:0)	251	139	0.55
Cer(d38:1)	790	348	0.44
Cer(d38:2)	1036	760	0.73
Cer(t38:1)	1856	1417	0.76
Cer(t44:0)	218	229	1.05
PI-Cer(t38:1)	213	151	0.71
MIPC(t38:1)	11	59	5.31
etc [2]			
Coenzyme Q10	6084	6016	0.99
Ergosteryl oleate	1115	612	0.55

Compounds higher or lower than 3 fold-change are shown in red or blue.

Supplemental movie 1

Time-lapse movie of living wild-type cells. Cells were first cultivated at 26°C, and then incubated further at 26°C in a microfluidic perfusion chamber with a continuous supply of EMM2 medium. Differential interference contrast (DIC) images were obtained at 15-min intervals and are shown at 8 frames / sec. The same cells are shown in Figure 2A (top).

Supplemental movie 2

Time-lapse movie of living *cwh43-G753R* mutant cells. Cells were first cultivated at 26°C, and then incubated further at 26°C in a microfluidic perfusion chamber with a continuous supply of EMM2 medium. Differential interference contrast (DIC) images were obtained at 15-min intervals and are shown at 8 frames / sec. The same cells are shown in Figure 2A (bottom).

Supplemental movie 3

Time-lapse movie of living wild-type cells. Cells were first cultivated at 26°C, and then shifted to 36°C in a microfluidic perfusion chamber with a continuous supply of EMM2 medium. Differential interference contrast (DIC) images were obtained at 15-min intervals and are shown at 8 frames / sec. The same cells are shown in Figure 2B (top).

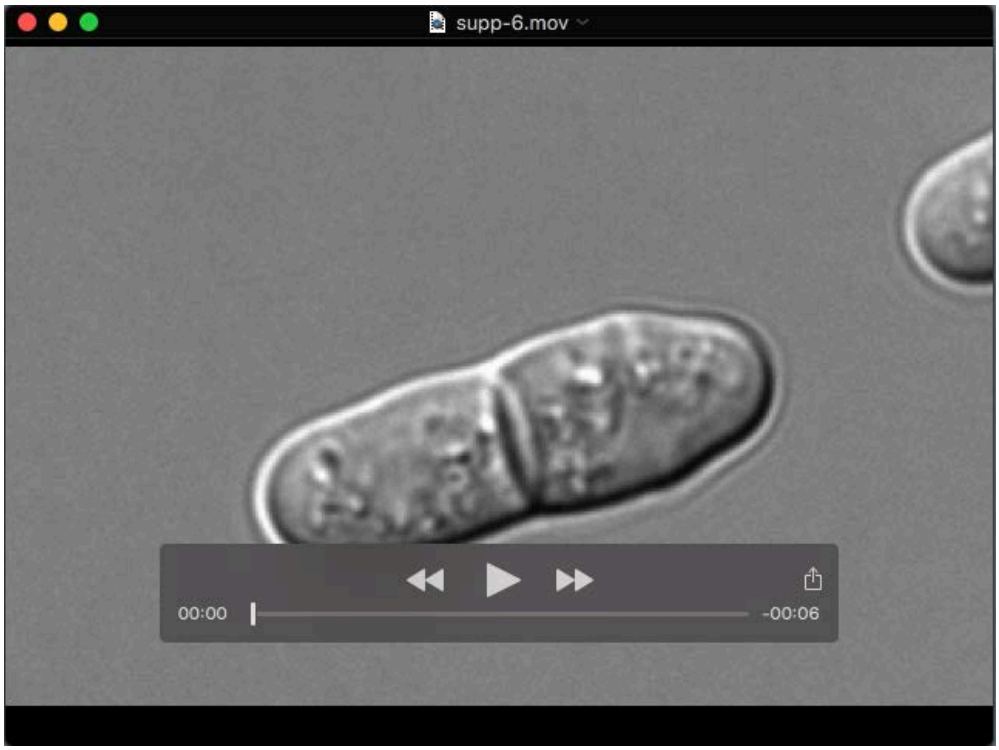

Supplemental movie 4

Time-lapse movie of living *cwh43-G753R* mutant cells. Cells were first cultivated at 26°C, and then shifted to 36°C in a microfluidic perfusion chamber with a continuous supply of EMM2 medium. Differential interference contrast (DIC) images were obtained at 15-min intervals and are shown at 8 frames / sec. The same cells are shown in Figure 2B (bottom).

References

Kawasaki, Y., Nagao, K., Nakamura, T. and Yanagida, M. (2006). Fission yeast MAP kinase is required for the increased securin-separase interaction that rescues separase mutants under stresses. Cell Cycle 5, 1831-1839.

Shimanuki, M., Uehara, L., Pluskal, T., Yoshida, T., Kokubu, A., Kawasaki, Y. and Yanagida, M. (2013). Klf1, a C2H2 zinc finger-transcription factor, is required for cell wall maintenance during long-term quiescence in differentiated G0 phase. PLoS ONE 8, e78545.